INVESTIGATING NON-FULLERENE ACCEPTORS IN ORGANIC PHOTOVOLTAICS

Nicole Bauer

A dissertation submitted to the faculty of the University of North Carolina at Chapel Hill in partial fulfillment of the requirements for the degree of Doctor of Philosophy in the Department of Chemistry.

Chapel Hill
2019

Approved by:

Joanna Atkin

Andrew Moran

Sergei Sheiko

Scott Warren

Wei You

ABSTRACT

Nicole Bauer: Investigating Non-Fullerene Acceptors in Organic Photovoltaics
(Under the direction of Wei You)

Organic photovoltaics are becoming a viable alternative to silicon solar technologies due to their lower cost and ease of fabrication. Recently, the rise of a new class of electron acceptor materials, known as non-fullerene acceptors (NFAs), has led to dramatic improvements in the performance of organic photovoltaics, reaching efficiencies over 15%. Despite these impressive improvements, the working mechanisms of these NFAs and their structure-property relationships are not well understood. In this dissertation, we investigated these new acceptors in an attempt to understand how their design influences their performance in an organic photovoltaic device. We first performed a comparative study of an NFA with a traditional fullerene derivative to determine how and why their performance differs. We found that the devices incorporating the NFA displayed a lower efficiency due to lower charge mobility and a less desirable film morphology, indicating that the crystallinity of an NFA is an important factor to consider. Then, we studied the effect of donor polymer fluorination on the performance of an NFA-based device, and found that fluorination improves the charge transport and extraction, as well as the bulk heterojunction morphology. These results demonstrate that, similar to fullerene-based systems, donor polymer fluorination is an effective method to improve device performance. Lastly, we studied the effect of simultaneous fluorination of the donor and NFA, as well as the degree of fluorination in the device. We found that fluorination of the NFA leads to an improved current and fill factor due to an extended absorption range and improved mobility and morphology.

Additionally, the device containing the most fluorine substituents achieved the highest efficiency. The insights gained from these studies can inform the design of new acceptor materials to obtain higher efficiencies and make polymer-based organic photovoltaics competitive for industrial processing.

ACKNOWLEDGEMENTS

First, I would like to thank my advisor, Dr. Wei You, for his support over the last five years. His optimism and guidance made all this work possible. I would also like to thank my committee, Dr. Joanna Atkin, Dr. Andrew Moran, Dr. Sergei Sheiko, and Dr. Scott Warren, for their time and support of this effort.

Second, I would like to thank Dr. Liang Yan for everything he has taught me about organic semiconductors, and always being willing to answer my questions and help when I needed it. I would also like to thank Dr. Qianqian Zhang and Jeromy Rech for making all of the polymers used in this work, I could not have done this without them. Additionally, I want to thank the other members of the You Group, past and present, for their help and for making the lab a fun and supportive place to work.

I would also like to thank our collaborators, Dr. Harald Ade, Dr. Xiaowei Zhan, Dr. He Yan, Dr. Franky So, and their students for making the acceptor materials used in this work and assisting with characterization and additional experiments.

I also thank all my family and friends, especially my parents. They have always supported me in whatever I chose to do, and I would not be where I am today without them.

Lastly, I would like to thank Dalton for his support through this effort, and for always being able to make me smile through the frustrating and stressful times.

TABLE OF CONTENTS

LIST OF TABLES

LIST OF FIGURES

LIST OF CHARTS

LIST OF ABBREVIATIONS

BHJ	Bulk heterojunction
BnDT	Benzo[1,2-b:4,5-b’]dithiophene
CuSCN	Copper thiocyanate
CT State	Charge transfer state
CV	Cyclic voltammetry
E_{CT}	Energy of the charge transfer state
EQE	External quantum efficiency
ETL	Electron transport layer
FF	Fill factor
FREA	Fused ring electron acceptor
FTAZ	5,6-difluoro-2-alkyl-4,7-di(thiophen-2-yl)-2*H*benzo[d][1,2,3]triazole
GIWAXS	Grazing incidence wide-angle X-ray scattering
HOMO	Highest occupied molecular orbital
HTAZ	2-alkyl-4,7-di(thiophen-2-yl)-2*H*benzo[d][1,2,3]triazole
HTL	Hole transport layer
IDTT	Indacenodithieno[3,2-b]thiophene
INCN	2-(3-oxo-2,3-dihydroinden-1-ylidene)malonitrile
ITIC	3,9-bis(2-methylene-(3-(1,1-dicyanomethylene)-indanone))-5,5,11,11-tetrakis(4-hexylphenyl)-dithieno[2,3-d:2’,3’-d’]-s-indaceno[1,2-b:5,6-b’]dithiophene
ITIC-Th	3,9-bis(2-methylene-(3-(1,1-dicyanomethylene)-indanone))-5,5,11,11-tetrakis(5-hexylthienyl)-dithieno[2,3-d:2’,3’-d’]-s-indaceno[1,2-b:5,6-b’]dithiophene

ITO	Indium-doped tin oxide
J_{sc}	Short-circuit current density
LUMO	Lowest unoccupied molecular orbital
NFA	Non-fullerene acceptor
OPV	Organic photovoltaic
PCBM	Phenyl-C61-butyric acid methyl ester
PCE	Power conversion efficiency
PDI	Perylene diimide
PEDOT:PSS	Poly(3,4-ethylenedioxythiophene):poly(styrenesulfonate)
PL	Photoluminescence
PSC	Polymer solar cell
PyCNTAZ	2-alkyl-4,7-di(thiophen-2-yl)-2*H*-[1,2,3]triazolo[4,5-c]pyridine
RSoXS	Resonant soft X-ray scattering
SCLC	Space charge limited current
SMA	Small molecule acceptor
TAZ	2-methyl-2*H*-benzo[d][1,2,3]triazole
V_{oc}	Open-circuit voltage

CHAPTER 1: INTRODUCTION

1.1 History and Introduction to Organic Photovoltaics

The increasing demand for clean, renewable energy has driven the development of new technologies for solar energy, such as organic photovoltaics (OPVs). OPVs have become a viable alternative to the widely produced silicon technologies due to their advantages such as lower cost and ease of processing. Additionally, OPVs can be semi-transparent and flexible, allowing them to be utilized in a wider variety of potential applications such as wearable electronics and smart windows.

In 1986, one of the first working OPV devices was reported by Tang *et al.*[1] The device utilized a bilayer structure of copper phthalocyanine as the donor material and a perylene diimide derivative as the acceptor material, and obtained a power conversion efficiency (PCE) of ~1%. A few years later, in 1992, Heeger *et al.* demonstrated ultrafast electron transfer from a conjugated polymer to a fullerene, beginning the era of fullerene-based OPVs.[2] Despite the efficient charge transfer in early bilayer devices, low efficiencies were observed due to the limited lifetime and short diffusion length of excitons. To combat this issue, Heeger *et al.* developed the bulk heterojunction (BHJ), an interpenetrating network of donor and acceptor domains with nanoscale phase separation that greatly increases the interfacial area between the electron donor and electron acceptor.[3] OPV devices utilizing the BHJ structure generally obtain much higher

efficiencies compared to those with a bilayer structure, due to improved exciton dissociation and electron transfer in the film.

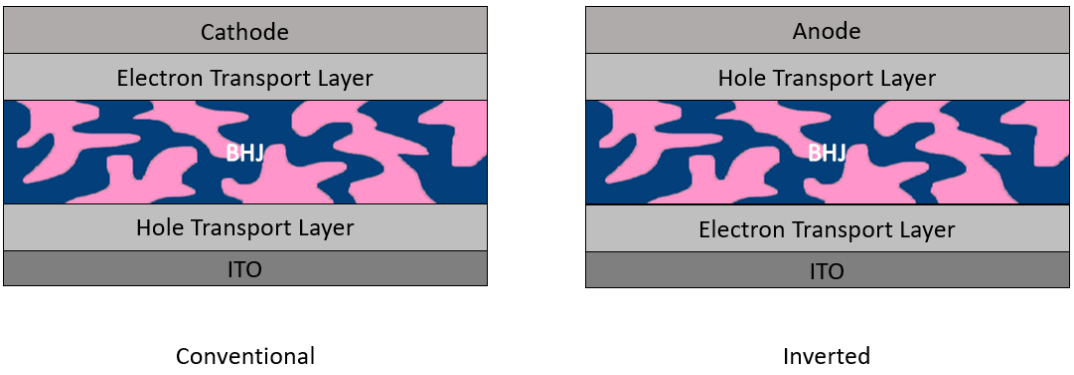

Figure 1.1 Typical architectures for BHJ-based organic photovoltaics

To improve charge transport and extraction for BHJ solar cells, researchers commonly utilize transport layers in addition to the electrodes and BHJ active layer. These transport layers allow for more selective transport of one charge carrier (electrons or holes) while blocking the other. Typical architectures for BHJ-based OPVs are displayed in **Figure 1.1**. Both configurations contain a transparent electrode, often indium-doped tin oxide (ITO), on the side which is irradiated. The conventional device often contains a hole transport layer (HTL) on top of the ITO, followed by the active layer which is composed of a BHJ of the electron donor and acceptor. The device is completed with an electron transport layer (ETL), often made of a low work-function metal such as calcium, and a top electrode generally composed of either aluminum or silver. The inverted device architecture is similar, but switches the position of the HTL and ETL. In this case, a high work function metal such as MoO_3 is often utilized as the HTL, providing a more air-stable device as MoO_3 does not oxidize as easily as calcium in air. In

order for highly efficient charge transfer to occur, each of these layers needs to have appropriate energy levels and work functions to allow for band alignment and Ohmic contact.

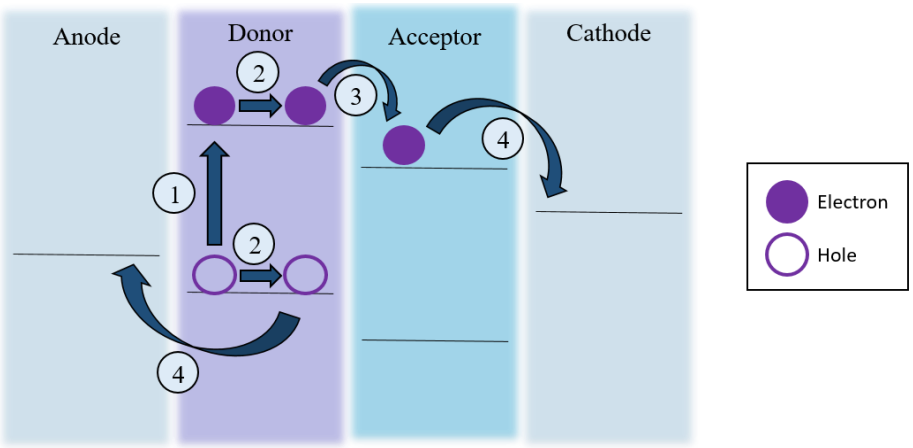

Figure 1.2 The four steps to charge collection in an OPV

Charge collection in an OPV can be split into four main steps: (1) exciton generation, (2) exciton diffusion, (3) charge separation, and (4) charge transport (**Figure 1.2**). In step (1), photons of appropriate energy are absorbed by the active layer (often by the donor polymer in a fullerene-based OPV) and an electron is excited from the highest occupied molecular orbital (HOMO) level to the lowest unoccupied molecular orbital (LUMO) level, leaving behind a positively charged hole. This electron-hole pair exists as a tightly bound Frenkel exciton due to the low dielectric constant of organic materials.[4] In step (2), the exciton diffuses to the donor-acceptor interface in the BHJ and the electron is transferred to the LUMO level of the acceptor, forming a charge transfer (CT) state. At this point, in step (3), the energy offset between the donor and acceptor allows the exciton to dissociate into free charge carriers, with the electron on the n-type acceptor material (i.e. fullerene) and the hole on the p-type donor (i.e. conjugated polymer). Lastly, in step

(4), the free charge carriers travel through their respective phases and are collected at the electrodes.

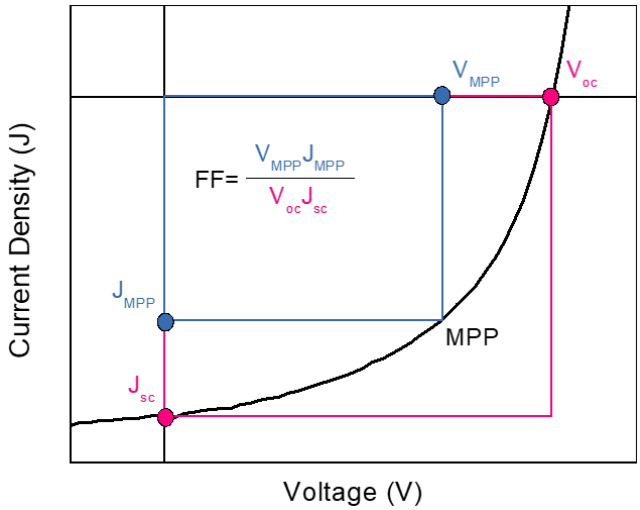

Figure 1.3 Characteristic current density-voltage (J-V) curve for an OPV

In order to judge the efficacy of an OPV, there are three primary parameters to consider: the short-circuit current density (J_{sc}), open-circuit voltage (V_{oc}), and fill factor (*FF*) (**Figure 1.3**). The J_{sc} is the maximum current density output from the device, while the V_{oc} is the maximum voltage. The *FF* is the ratio between the measured maximum power point (MPP) in the device and the theoretical MPP determined by the product of the J_{sc} and V_{oc}. The product of these three parameters divided by the incident power (P_{in}) gives the power conversion efficiency (PCE), which is the main figure of merit for OPVs (Equation 1.1).

$$\mathrm{PCE} = \frac{V_{oc} \times J_{sc} \times FF}{P_{in}} \qquad (1.1)$$

The J_{sc}, V_{oc}, and *FF* are dependent on a variety of intrinsic properties of the donor and acceptor materials, as well as the device fabrication conditions. For example, the J_{sc} can be affected by properties such as the band gap of the materials, light absorption, charge mobility, and active layer thickness, while the *FF* is dependent on properties such as the charge recombination and morphology. Finally, the V_{oc} is dependent on the energy of the CT state, which is generally proportional to the difference between the HOMO level of the donor and the LUMO level of the acceptor.

1.2 Donor Polymer Design

While the donor material in an OPV can be either a small molecule or conjugated polymer, this dissertation will only focus on conjugated polymer donors. Over the past years, there has been a lot of research done to better understand the structure-property relationships of conjugated polymers. When designing a conjugated polymer for use in OPVs, there are three main components to consider: the backbone, the side chains, and the substituents. The backbone plays a major role in determining properties such as the energy levels, band gap, and intra- and intermolecular interactions, which are extremely important in determining a polymer's performance in an OPV. Side chains are important to consider as well, as they affect the solubility and processability of the polymer, as well as the intermolecular interactions between polymer chains and the interactions between the polymer and the electron acceptor. Lastly, substituents (such as fluorine atoms) can be added along the backbone to fine tune the physical and electronic properties of the polymer.[5]

While the early generations of donor polymers consisted of a single repeating unit, for example thiophene in P3HT, the design of current high performance polymers consists of more

complex architectures. The majority of polymers designed for OPVs utilize a "donor-acceptor" (D-A) structure, where the repeat unit consists of an electron-rich donor moiety linked to an electron-poor acceptor moiety. This D-A structure promotes increased planarity of the backbone to facilitate internal charge transfer and electron delocalization between the donor and acceptor moieties, which decreases the bandgap and allows for more light absorption. Additionally, D-A polymers typically display localized HOMO and LUMO levels on the donor and acceptor moiety, respectively. By adjusting the electron-donating ability of the donor moiety or the electron-withdrawing ability of the acceptor moiety, the HOMO and LUMO levels of the polymer can be independently tuned. It is important to note that while these polymers have both a donor and acceptor moiety, they are still an electron donor material.

Fluorine is a commonly used substituent to improve the performance of a polymer in an OPV. As Chapters 3 and 4 will focus on the impact of fluorination, we will give a brief introduction to this "fluorine effect." Due to its small atomic radius, fluorine can be added along the polymer backbone to tune the optoelectronic properties without introducing the steric hindrance associated with many other substituents. Additionally, the electron-withdrawing properties of fluorine from its high electronegativity allow it to lower both the HOMO and LUMO levels of a polymer, which can increase the V_{oc} without having a major effect on the bandgap and the J_{sc}. Additionally, fluorine can increase the planarity of the backbone through non-covalent (e.g., F···H, F···S, F···π) intramolecular interactions and promote aggregation of the polymer chains, which is beneficial for charge transport. Fluorine can been added to many positions along a polymer chain, including the donor moiety, acceptor moiety, side chains, and π-linker groups. However, due to its electron-withdrawing nature it is most commonly added to the acceptor moiety. The position of the fluorine atom, as well as the number of fluorine

substituents, have a large effect on the performance of the polymer in an OPV. While fluorine substituents do often lead to an improvement in the PCE, there are some instances in which the position or number of the substituents can decrease the performance.[6]

1.3 Introduction to Non-Fullerene Acceptors

As mentioned above, fullerene and its derivatives were the most commonly used acceptors for OPVs due to their high electron mobility, electron affinity, and ability to form a favorable morphology with a variety of donor polymers. Despite these advantages, however, fullerenes absorb very little visible light and have relatively fixed energy levels, limiting the polymers they can be paired with to form a working device. Additionally, fullerenes tend to aggregate in a thin film over time, causing an unstable morphology that can have a negative effect on the PCE. Recently, non-fullerene acceptors (NFAs) have emerged as a promising alternative to fullerene derivatives as electron acceptors. Although NFAs can be both n-type semiconducting polymer and small molecule acceptors, the term NFA is generally associated with an acceptor-donor-acceptor (A-D-A) type fused-ring small molecule acceptor. These A-D-A acceptors may also be referred to as small molecule acceptors (SMAs) or fused ring electron acceptors (FREAs). NFAs allow for easier tuning of optical and electronic properties than fullerene derivatives, and can be matched to a wide variety of donor polymers. NFAs generally have stronger light absorption than fullerenes, allowing them to contribute to exciton generation in a device and increase the J_{sc}, especially if their absorption is complementary to that of the donor polymer. Additionally, the LUMO level of the NFA can be tuned to increase the $LUMO_{Acceptor}$-$HOMO_{Donor}$ gap and, therefore, the V_{oc}.

Early NFAs were comprised of a wide variety of chemical structures, including building blocks such as phthalocyanines and rylenes, among others.[7,8] One of the most commonly used structures was perylene diimide (PDI) due to its high electron mobility, high electron affinity, and variety of sites for functionalization. PDI-based molecules also exhibit a strong tendency for π-π stacking between molecules, which is beneficial for charge transport in an OPV. However, this stacking tendency can also lead to crystallites which are too large for a favorable BHJ morphology, which can hinder exciton dissociation.[7] Due to this crystallite formation, designing an efficient PDI-based NFA is a challenging prospect.

More recently, there has been movement away from the large PDI acceptor moiety to the smaller electron-withdrawing ending IC unit (i.e., 1,1-dicyanomethylene-3-indanone). These IC units are often connected to fused-ring ladder core like indacenodithienothiophene (IDTT).[9] This design was popularized in 2015 when Lin *et al.* introduced a new FREA named ITIC, which, when paired with the donor polymer PTB7-Th, gave a PCE of 6.80%, the highest for NFA-based OPVs at the time.[10] Since this report, the ITIC structure has become a commonly used building block for new FREAs, as many research groups have altered the side chains and substituents to yield even higher PCEs.[9] With the introduction of FREAs such as ITIC, the efficiencies of NFA-based OPVs have surpassed those based on fullerene derivatives, and have recently exceeded 15%.[11]

CHAPTER 2: COMPARING NON-FULLERENE ACCEPTORS WITH FULLERENE IN POLYMER SOLAR CELLS: A CASE STUDY WITH FTAZ AND PYCNTAZ[1]

2.1 Introduction

Organic photovoltaics (OPVs) are promising candidates for solar energy applications for reasons including potentially low fabrication cost (from both a processing and a materials' perspective), light weight, and mechanical flexibility of the devices when compared to silicon solar cells. The most common electron acceptors used in OPVs are fullerene derivatives because of their high electron affinity and relatively high electron mobility.[12] Despite these advantages, fullerenes have a number of drawbacks, including difficult synthesis, rather fixed energy levels, and poor light absorption in the visible region. To address these fullerene-associated issues, non-fullerene acceptors (NFAs) have gained significant momentum in recent years, due to their many advantages over traditional fullerenes.[13] For example, one can easily tune the optical and electronic properties of NFAs via molecular design, which could allow for enhanced open-circuit voltage (V_{oc}) from their energy levels matching those of the donor polymer [14,15] and increased current (J_{sc}) from their complementary absorption to that of the donor polymer.[16,17] Benefitting from the experiences gained and lessons learned from decades of research on fullerene-based bulk heterojunction (BHJ) systems, the community has made rapid progress in the past two years

[1] Reprinted with permission from Bauer, N.; Zhang, Q.; Zhao, J.; Ye, L.; Kim, J-H.; Constantinou, I.; Yan, L.; So, F.; Ade, H.; Yan, H.; You, W. *J. Mater. Chem. A*, **2017**, *5*, 4886-4893

with record high efficiency reaching ~12% for NFA-based devices,[18,19] on par with the highest efficiency achieved for fullerene blends.[20–22]

Though a higher V_{oc} is usually obtained for NFA-based organic solar cells than that of their fullerene-based counterparts, the NFA-based devices often suffer from a noticeably reduced short-circuit current (J_{sc}) and/or fill factor (*FF*).[23] Since both J_{sc} and *FF* are closely related to the loss mechanisms in photovoltaic devices (e.g., bimolecular recombination),[24,25] it is important to understand such loss mechanisms in NFA-based solar cells, ideally in a comparative manner with the corresponding solar cells based on fullerenes. Unfortunately, such studies have only begun to emerge.[26,27]

We set our study by first choosing SF-PDI_2 as the small molecule, non-fullerene electron acceptor. In a previous study by Zhao et al., SF-PDI_2 was paired with the polymer donor PffBT4T-2DT and achieved a high V_{oc} of 0.98 V in their BHJ devices, leading to a respectable power conversion efficiency (PCE) of 6.3%.[28] We then selected two TAZ-based donor polymers, FTAZ and PyCNTAZ (structures given in **Chart 2.1**), that have shown impressive device performance in their BHJ solar cells based on fullerene acceptors.[29,30] The first donor polymer, FTAZ, containing a fluorinated benzotriazole as the electron-accepting moiety, was reported by Price et al. in 2011.[29] They obtained a relatively high V_{oc} of 0.79 V with an impressive *FF* of 72%, giving an overall PCE of over 7%.[25,31] The other donor polymer chosen for this work, PyCNTAZ, was introduced by Li et al. in 2015.[30] In BHJ solar cells with PCBM, PyCNTAZ displayed a V_{oc} of 0.96 V, higher than that of FTAZ, leading to a higher PCE of 8.37% at an optimized active layer thickness of 300 nm.

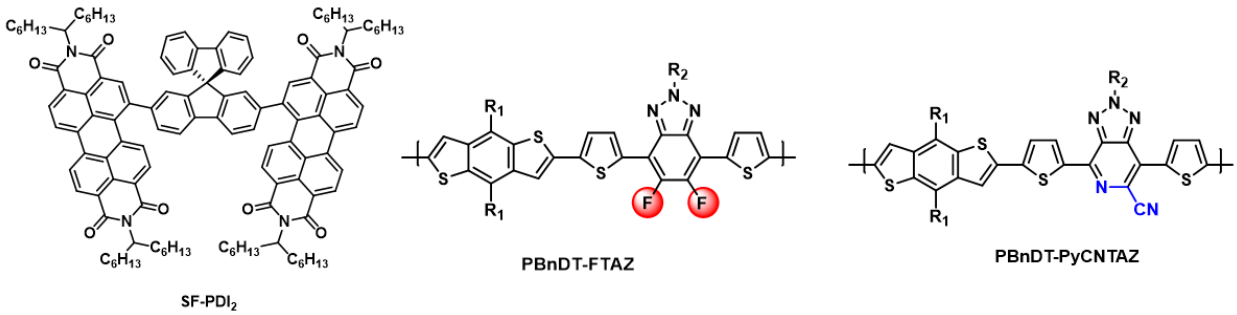

Chart 2.1 Chemical structures of SF-PDI_2, FTAZ, and PyCNTAZ

In this study, we aim to directly compare the photovoltaic performance of four BHJ blends based on two acceptors (SF-PDI_2 and $PC_{61}BM$, referred to here as PCBM) and two donor polymers (FTAZ and PyCNTAZ), and investigate the device physics and morphology to determine the origins of the differences in performance. Notably, for both polymers, the SF-PDI_2-based photovoltaic device has a higher V_{oc} than that of the PCBM-based counterpart. This higher V_{oc} is directly correlated with the higher charge transfer state energy (E_{ct}) of the SF-PDI_2 blend, mainly due to the higher-lying lowest unoccupied molecular orbital (LUMO) level of SF-PDI_2. However, the SF-PDI_2-based device displays a lower *FF* than that of the PCBM-based device due to a mobility imbalance and less pure domains. Furthermore, the SF-PDI_2-based device shows a lower J_{sc}, which can be ascribed to inefficient charge transfer from the donor polymer to the non-fullerene acceptor (i.e., SF-PDI_2) and increased non-geminate recombination in such non-fullerene acceptor-based blends.

2.2 Results and Discussion

2.2.1 Photovoltaic Performance

To investigate the performance differences displayed between devices containing a fullerene and a non-fullerene acceptor, the small molecule acceptor SF-PDI_2 was paired with the donor polymers FTAZ and PyCNTAZ in bulk heterojunction (BHJ) solar cells. Devices were also fabricated using PCBM as the acceptor with both polymers for comparison. A conventional device configuration was used (ITO/HTL/Active Layer/Ca/Al), where the hole transport layer (HTL) was poly(3,4-ethylenedioxythiophene)-poly(styrenesulfonate) (PEDOT:PSS) for FTAZ-based devices and copper thiocyanate (CuSCN) for PyCNTAZ-based devices. Due to the deeper HOMO (highest occupied molecular orbital) level of PyCNTAZ, using CuSCN as HTL can help improve the photovoltaic device performance when compared to PEDOT:PSS as HTL, as we previously demonstrated.[30] Active layer thicknesses for all four devices were kept at ~150 nm to minimize thickness effects on performance, and the donor:acceptor (D:A) ratio in the BHJ blend for all devices was 1:2 by weight. The *J-V* curves are shown in **Figure 2.1a** and the photovoltaic characteristics are summarized in **Table 2.1**. For the SF-PDI_2 blends, the PyCNTAZ-based device displays a higher J_{sc} than the FTAZ-based device, which can be ascribed to less overlapping/more complementary absorption of PyCNTAZ and SF-PDI_2 (**Figure 2.1b**) and efficient utilization of both components to generate current. Pleasingly, when compared to the fullerene-based device, the SF-PDI_2-based device gives a higher V_{oc} value for both polymers than the PCBM-based one, i.e., 0.935 V vs. 0.846 V for FTAZ:SF-PDI_2 and FTAZ:PCBM, respectively, and 1.152 V vs. 0.975 V for PyCNTAZ:SF-PDI_2 and PyCNTAZ:PCBM, respectively. However, the SF-PDI_2-based device has a lower J_{sc} and *FF* than those of the PCBM-based device, leading to a lower power conversion efficiency (PCE) by the former device

for both polymers. Below, we will discuss each device characteristic in further detail and strive to identify the underlying reasons for the observed trends.

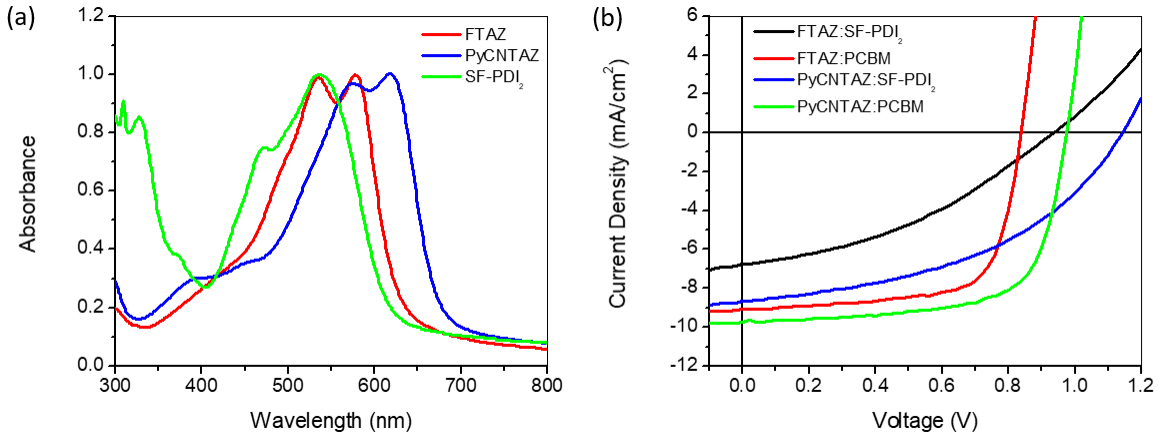

Figure 2.1 a) J-V characteristics of SF-PDI_2- and PCBM-based solar cells; b) Normalized absorption spectra of neat FTAZ, PyCNTAZ, and SF-PDI_2 films

Table 2.1 Photovoltaic characteristics of SF-PDI_2- and PCBM-based solar cells

Blend	J_{sc} (mA/cm^2)	V_{oc} (V)	FF (%)	PCE (%)
FTAZ:SF-PDI_2	6.70±0.29	0.935±.005	36.7±1.6	2.30±0.15
FTAZ:PCBM	9.16±0.32	0.846±.007	73.3±2.0	5.68±0.23
PyCNTAZ:SF-PDI_2	8.15±0.12	1.152±0.003	46.5±1.3	4.37±0.17
PyCNTAZ:PCBM	10.10±0.38	0.975±0.003	64.8±2.3	6.39±0.41

2.2.2 Open-Circuit Voltage (V_{oc})

To determine the cause of the higher V_{oc} for SF-PDI_2-based devices, we first considered the energy levels of the donors and acceptors. Such values can be extracted from previous reports,[28–30,32] which are presented in **Figure 2.2**. It has long been argued that V_{oc} is primarily proportional to the difference between the LUMO energy level of the acceptor and the HOMO energy level of the donor, if Ohmic contacts are achieved at both cathode and anode interfaces. SF-PDI_2 has a higher-lying LUMO level than PCBM, –3.83 eV compared to –4.07 eV, respectively. This difference (~ 0.2 eV) certainly accounts for a higher V_{oc} for both SF-PDI_2-based solar cells; yet the observed V_{oc} difference (~ 0.09 V for FTAZ-based devices and ~ 0.15 V for PyCNTAZ-based devices) needs further investigation (*vide infra*).

Table 2.2 V_{oc}, E_{CT}, and energetic losses for FTAZ- and PyCNTAZ-based solar cells

Blend	**V_{oc} (V)**	**E_{opt} (eV)**	**E_{ct} (eV)**	**ΔE (eV)** E_{opt}-V_{oc}	**ΔE_{CS} (eV)** E_{opt}-E_{ct}	**ΔE_{NG} (eV)** E_{ct}-V_{oc}
FTAZ:SF-PDI_2	0.93	1.99	1.55	1.06	0.44	0.62
FTAZ:PCBM	0.77	1.66	1.39	0.89	0.27	0.62
PyCNTAZ:SF-PDI_2	1.10	1.80	1.76	0.70	0.04	0.66
PyCNTAZ:PCBM	0.97	1.66	1.63	0.69	0.03	0.66

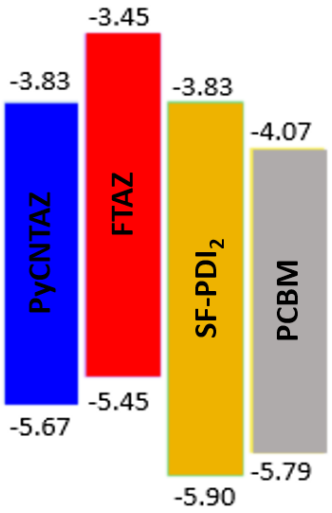

Figure 2.2 HOMO and LUMO levels of PyCNTAZ, FTAZ, SF-PDI_2, and PCBM

Vandewal et al demonstrated that V_{oc} is primarily determined by the interfacial charge-transfer (CT) states between the donor and the acceptor, with additional loss coming from the radiative emission and non-radiative emission.[33,34] Equation 2.1 presents the relationship,

$$V_{oc} = \frac{kT}{q} ln\left(\frac{J_{ph}}{J_0} + 1\right) = \frac{E_{CT}}{q} + \frac{kT}{q} ln\left(\frac{J_{sc} h^3 c^2}{f q 2\pi (E_{CT} - \lambda)}\right) + \frac{kT}{q} ln(EQE_{EL}) \quad (2.1)$$

which can also be re-written as (q is the elementary charge, i.e., e)

$$eV_{oc} = E_{CT} + kTln\left(\frac{J_{sc} h^3 c^2}{f q 2\pi (E_{CT} - \lambda)}\right) + kTln(EQE_{EL}) \quad (2.2)$$

According to Faist et al,[35] the energy difference between eV_{oc} and E_{CT} is the loss due to the non-geminate recombination (i.e., $\Delta E_{NG} = E_{CT} - eV_{oc}$), and the charge separation energy/exciton splitting energy ($\Delta E_{CS} = E_{opt} - E_{CT}$) is the difference between the optical gap (E_{opt}) and the

energy of the CT state manifold. Unlike a typical inorganic solar cell where there are essentially no CT states (thus $\Delta E_{CS} \sim 0$), the presence of the CT state manifold constructs a significant channel of energy loss (ΔE_{CS}), manifested by the typically observed smaller V_{oc} when compared with the band gap (i.e., $eV_{oc} = E_{opt} - \Delta E_{CS} - \Delta E_{NG}$). Experimentally, high sensitivity external quantum efficiency (EQE) measurements were performed and the resulting spectra (**Figure 2.3**) were fitted to obtain an estimate for E_{CT} (**Table 2.2**) using Equation 2.3.[32]

$$EQE\ (E) \propto \frac{1}{E\sqrt{4\pi\lambda kT}} \exp\left(-\frac{(E_{CT}+\lambda-E)^2}{4\lambda kT}\right) \tag{2.3}$$

With optically determined band gap (E_{opt}) and measured V_{oc}, the aforementioned ΔE_{CS} and ΔE_{NG} can thereby be determined for each blend (**Table 2.2**).

For both polymers, the difference in E_{CT} between the fullerene and non-fullerene device is almost identical to the difference in V_{oc} (numerically), for example, ΔE_{CT} of 0.15 eV (1.55 – 1.39) vs. ΔV_{oc} of 0.16 (0.93 – 0.77) for FTAZ. This observation implies that the V_{oc} loss in these systems is independent of the choice of acceptor (i.e., SF-PDI$_2$ or PCBM). Furthermore, ΔE_{NG} is similar for all devices at ~ 0.6 eV, indicating that V_{oc} losses from non-geminate recombination are also very similar in all four blends. However, while the charge separation energy (ΔE_{CS}) for FTAZ-based cells is 'normal', 0.27 eV for FTAZ:PCBM and 0.44 eV for FTAZ:SF-PDI$_2$, the PyCNTAZ-based devices display exceptionally low driving forces (ΔE_{CS}) of ~ 0.03 eV for both devices. While not as common, devices that maintain efficient charge separation and high performance but display a low ΔE_{CS} have been recently reported, interestingly, also for SF-PDI$_2$-based devices.[36] This exciting discovery certainly warrants further investigation, since achieving a low ΔE_{CS} is a very promising approach to further enhance the efficiency of polymer solar cells.

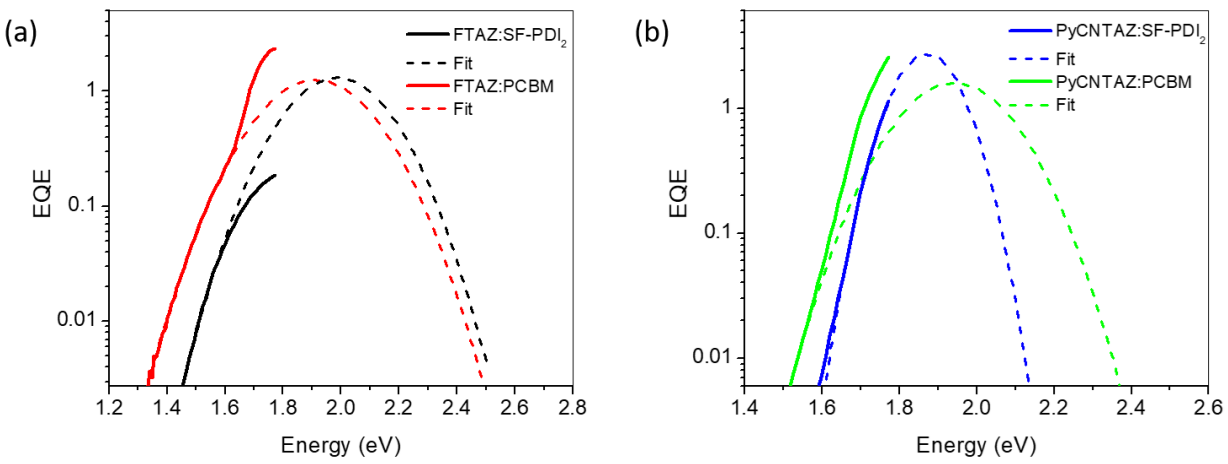

Figure 2.3 Measured low energy external quantum efficiency (EQE) curves and calculated fittings for a) FTAZ and b) PyCNTAZ based solar cells

2.2.3 Short-Circuit Current (J_{sc})

Comparing the J_{sc} values in **Table 2.1** raises one important question we try to answer with this study: why is J_{sc} lower in both cases for SF-PDI$_2$-based devices when compared with PCBM-based devices? In fact, there are multiple possible causes which can occur at various stages of the photovoltaic process (i.e., charge generation, charge transport and charge collection), to account for a lowered J_{sc}. For example, insufficient exciton quenching could lead to insufficient charge generation, and bimolecular recombination could compete with charge transport to the electrode, to name a few.

We first measured the photoluminescence (PL) quenching to study exciton splitting/*charge generation* in the BHJ blends, and the data is presented in **Figure 2.4**. Due to the absorption overlap of SF-PDI$_2$ with the two donor polymers, we chose to use D:A=10:1 to allow for quantitative determination of PL quenching (PL quenching with D:A=1:2 in **Figure A3**). It is clear from the results that SF-PDI$_2$-based blends show less PL quenching than that of PCBM-

based blends (for both FTAZ and PyCNTAZ), indicating that there may be an issue with donor to acceptor charge transfer in the SF-PDI_2-based systems, especially for PyCNTAZ. Incomplete charge transfer in the device would decrease the J_{sc} at the source of charge generation. For the FTAZ-based blends (**Figure 2.4a)**, the amount of quenching was 82% and 96% for FTAZ:SF-PDI_2 and FTAZ:PCBM, respectively, suggesting that the driving force (ΔE_{CS} > 0.2 eV) is large enough to allow only 10% acceptor to sufficiently quench the PL of FTAZ with either SF-PDI_2 or PCBM. On the other hand, for PyCNTAZ-based blends (**Figure 2.4b**), the amount of quenching was only 34% and 81% for PyCNTAZ:SF-PDI_2 and PyCNTAZ:PCBM, respectively. It is possible that due to the low driving force (ΔE_{CS} ~ 0 eV) of the PyCNTAZ blends, energy transfer may also play an important role in the PL quenching, in addition to photo-induced charge transfer. In the PyCNTAZ:PCBM blend, though the driving force is small (ΔE_{CS} ~ 0 eV), PCBM has a smaller band gap and there can be both energy transfer and charge transfer in the PyCNTAZ:PCBM system. Thus, ~ 10% PCBM is still able to quench a much larger degree of the PL of PyCNTAZ (**Figure 2.4b**). However, in the PyCNTAZ:SF-PDI_2 blend, there is essentially no energy transfer for quenching the PL of PyCNTAZ because the band gap of SF-PDI_2 is larger than that of PyCNTAZ; thus, the PL quenching is purely dependent upon the photo-induced charge transfer for the PyCNTAZ:SF-PDI_2 blend, which is not sufficient due to low driving force (ΔE_{CS} ~ 0 eV).

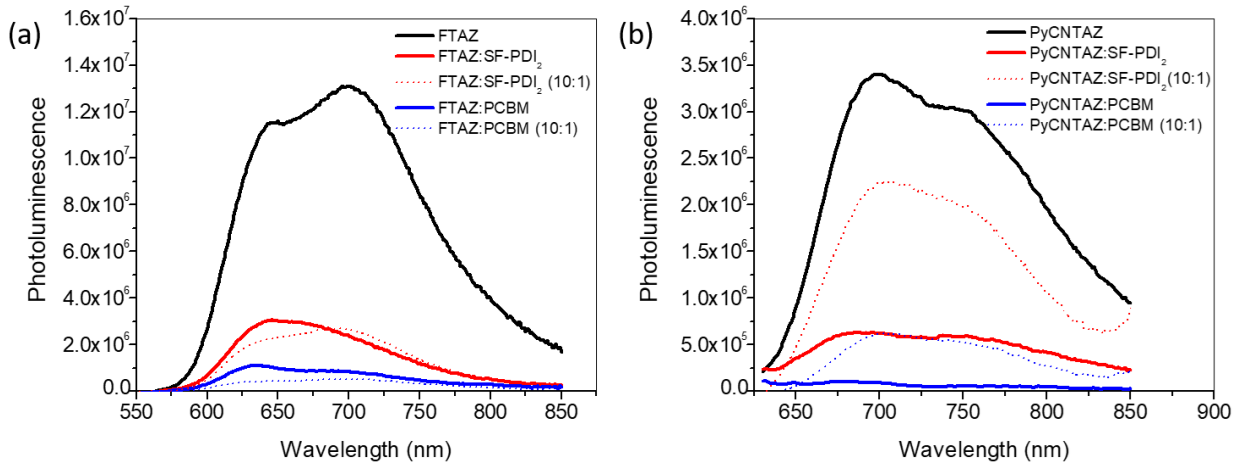

Figure 2.4 Photoluminescence of neat a) FTAZ (excitation at 532 nm) and b) PyCNTAZ (excitation at 618 nm) films and the blend films with SF-PDI$_2$ and PCBM (D:A=10:1)

We next attempted to probe the recombination mechanisms occurring in these devices, since the recombination, in particular the bimolecular recombination, is known to have a strong impact on *charge transport*. To this end, light intensity dependence of J_{sc} and V_{oc} were measured for the four devices. On the one hand, J_{sc} is known to have a power law dependence on light intensity, following the relation

$$J_{sc} \propto I^{\alpha} \tag{2.4}$$

where I is the light intensity and α is the slope of the log-log plot of J_{sc} vs intensity.[37] An α value close to unity is indicative of weak bimolecular recombination at short-circuit condition. The log plot of J_{sc} vs light intensity is displayed in **Figure 2.5a**. For both polymers, the α value for the fullerene-based device is closer to one than that of the non-fullerene device, suggesting increased bimolecular recombination in the SF-PDI$_2$-based devices at short-circuit. The increased

recombination would compete with charge extraction and lead to a lower current in the non-fullerene based devices.

On the other hand, when bimolecular recombination is the only loss mechanism, V_{oc} can be related to light intensity by the following equation

$$V_{oc} = \frac{E_{gap}}{q} - \frac{kT}{q} \ln\left[\frac{(1-P_D)\gamma N_C^2}{P_D G}\right] \quad (2.5)$$

where E_{gap} is the $HOMO_{Donor} - LUMO_{Acceptor}$ difference, k is the Boltzmann constant, T is the temperature in Kelvin, q is the elementary charge (i.e., e), P_D is the dissociation probability of electron-hole pairs, γ is the recombination constant, N_C is the effective density of states, and G is the generation rate of bound electron-hole pairs.[37] In this equation, G is proportional to the light intensity, and a semi-log plot of V_{oc} vs light intensity will yield a slope of kT/q if bimolecular recombination is the sole loss mechanism. **Figure 2.5b** presents the V_{oc} vs light intensity data for all four devices. For both polymers, the PCBM-based blends have a slope very close to kT/q, indicating that bimolecular recombination is the major loss mechanism at open-circuit condition in these devices. However, the FTAZ:SF-PDI_2 device shows a slope greater than kT/q whereas PyCNTAZ:SF-PDI_2 has a slope less than kT/q. These results indicate that the FTAZ:SF-PDI_2 device suffers from a combination of trap-assisted and bimolecular recombination at open-circuit condition,[38,39] while PyCNTAZ:SF-PDI_2 is mainly affected by surface recombination.[40,41] Due to these additional recombination channels, the number of charges that can successfully traverse the active layer and make it to the electrode will be less for the SF-PDI_2-based devices compared to the PCBM-based ones, which would decrease the current.

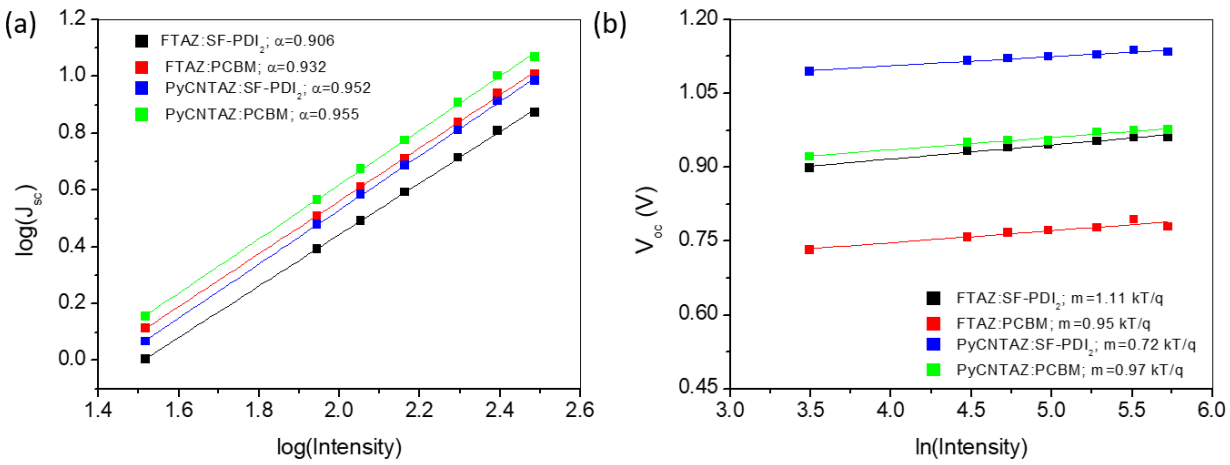

Figure 2.5 Light intensity dependence of a) short-circuit current and b) open-circuit voltage

Lastly, we studied the *charge collection* by comparing the charge collection probability, $P(E,T)$, for all blends. Experimentally, the photocurrent density (J_{ph}) was first measured as a function of the effective voltage V_{eff} (**Figure 2.6a**) for each device. J_{ph} is defined as J_L-J_D, where J_L is the current density under illumination and J_D is the current density in the dark, and V_{eff} is V_0-V, where V_0 is the voltage at which J_{ph}=0.[42,43] The photocurrent density (J_{ph}) was then used to calculate the charge collection probability, $P(E,T)$, for each blend using the equation

$$P(E,T) = \frac{J_{ph}}{J_{ph,sat}} \tag{2.6}$$

where $J_{ph,sat}$ is the saturated photocurrent density in the device.[43] At short-circuit condition, the PCBM-based devices have a higher $P(E,T)$ than the non-fullerene devices, 92.4% compared to 73.5% for FTAZ:PCBM and FTAZ:SF-PDI$_2$, respectively, and 89.3% compared to 79.8% for PyCNTAZ:PCBM and PyCNTAZ:SF-PDI$_2$, respectively. These results indicate that the charge

collection process is more efficient in the fullerene devices, which contributes to the higher J_{sc} of the fullerene-based devices for both polymers.

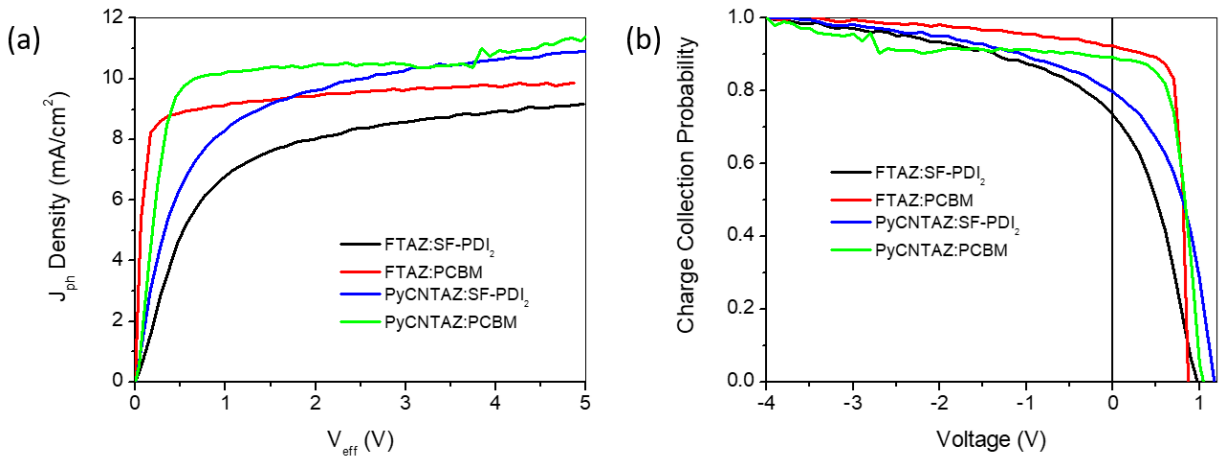

Figure 2.6 a) Photocurrent density and b) charge collection probability (P(E,T)) of SF-PDI$_2$- and PCBM-based solar cells

2.2.4 Fill Factor (FF)

We previously showed that the main reason for the unusually high *FF* of the FTAZ:PCBM device was the high hole mobility (1.2×10^{-3} cm^2 V^{-1} s^{-1}) and the balanced mobility (i.e., electron mobility on the same order of magnitude, ~ 5×10^{-3} cm^2 V^{-1} s^{-1}).[25] Indeed, the space-charge limited current (SCLC) mobilities for the PCBM-based devices in this study further confirmed the balanced mobilities (**Table 2.3**) for both polymers.

However, when switching out PCBM for SF-PDI$_2$, the SF-PDI$_2$-based devices show a large imbalance in the electron and hole mobility for both polymers (**Table 2.3**). Proctor et al. have previously shown that low and imbalanced mobilities can reduce the fill factor of a solar cell.[44] In our case, the hole mobility of the non-fullerene devices is one order of magnitude larger than

the electron mobility; this large mobility imbalance is likely a major cause of the decreased *FF* in the SF-PDI_2-based devices.

In addition to the mobility imbalance, the SF-PDI_2-based devices also display lower mobilities overall, in particular, for the electrons (on the order of 10^{-5} cm^2 V^{-1} s^{-1}). This may be due to the morphology of the SF-PDI_2-based films, which will be discussed in more detail in the next section. The low, imbalanced mobilities can lead to a build-up of space charge and exacerbate the charge transport via increased bimolecular recombination. This agrees with the results of the light intensity measurements, which indicate that the SF-PDI_2-based devices suffer from more recombination than the PCBM-based devices. The increased recombination would not only decrease the J_{sc} as mentioned previously, it would also have a negative effect on the *FF* for the non-fullerene based devices.

Table 2.3 Electron and hole mobilities for SF-PDI_2- and PCBM-based solar cells

Blend	Electron Mobility (cm^2 V^{-1} s^{-1})	Hole Mobility (cm^2 V^{-1} s^{-1})
FTAZ:SF-PDI_2	3.68E-5 ± 7.38E-6	6.35E-4 ± 2.19E-4
FTAZ:PCBM	1.68E-3 ± 5.65E-4	4.23E-3 ± 3.33E-3
PyCNTAZ:SF-PDI_2	1.88E-5 ± 2.53E-6	5.04E-4 ± 1.36E-4
PyCNTAZ:PCBM	2.28E-3 ± 1.43E-3	1.26E-3 ± 5.15E-4

2.2.5 Morphology

The morphology of BHJ thin films offers important information to further understand the observed photovoltaic behavior of these thin film based devices. To determine the molecular packing within the neat and blend films, grazing incidence wide-angle X-ray scattering (GIWAXS) measurements were performed. The scattering signatures of neat FTAZ and PyCNTAZ films are very similar, and both exhibit clear (100) peaks at q= 0.3 Å^{-1} in the in-plane direction and (010) peaks located at q=1.7 Å^{-1} in the out-of-plane direction (**Figure 2.7a-b**), suggesting the polymers have a face-on orientation with respect to the substrate. Such face-on feature was frequently observed before in many high-performance conjugated polymers and considered to be advantageous for hole transport across the active layer.[45] As shown in **Figure 2.7c**, the neat SF-PDI$_2$ film does not display a (010) reflection peak; rather, it shows weak (100) diffuse rings and an amorphous halo around q=1.3 Å^{-1} without a clear orientation preference.

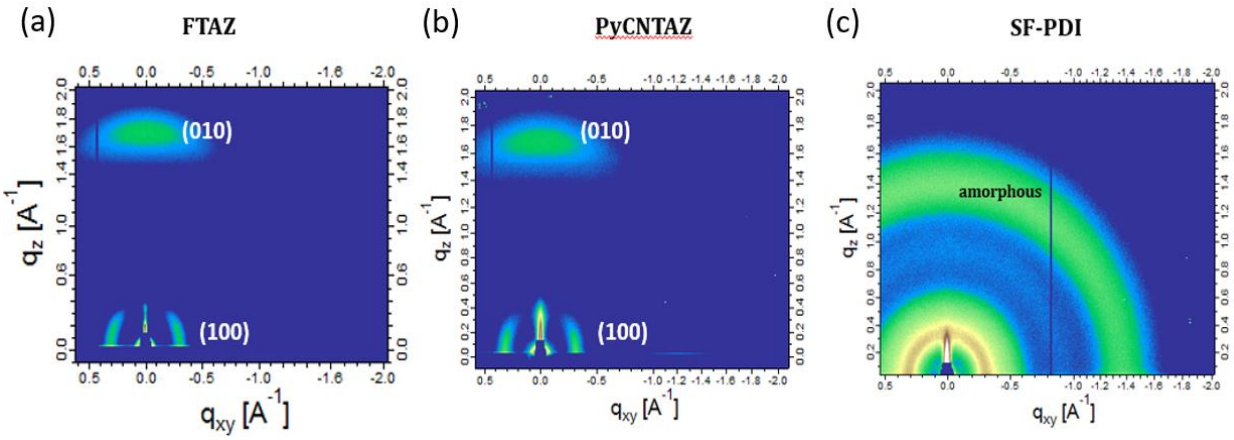

Figure 2.7 GIWAXS 2D patterns of the thin films based on neat materials: a) FTAZ; b) PyCNTAZ; c) SF-PDI$_2$

Shown in **Figure 2.8a-d** are the 2D GIWAXS patterns of these polymers blended with PCBM or SF-PDI$_2$. The SF-PDI$_2$-based blend films display weak (100) and (010) diffraction peaks, indicative of poor lamellar packing and π-π stacking. In contrast, the PCBM-based blends exhibit more clear lamellar (100) and (200) peaks, and (010) peak in the out-of-plane direction in addition to an isotropic ring located at q= 1.35 Å^{-1}, which is originated from pure PCBM aggregates.[46] Comparison of the GIWAXS patterns between fullerene and SF-PDI$_2$-based films indicates that the PCBM-based films are more ordered, which agrees well with the higher hole/electron mobility observed for these PCBM-based devices (**Table 2.3**). A higher degree of molecular ordering in the film could afford improved charge transport and thus higher charge mobility, leading to the higher J_{sc} and *FF* values measured for the PCBM-based devices.

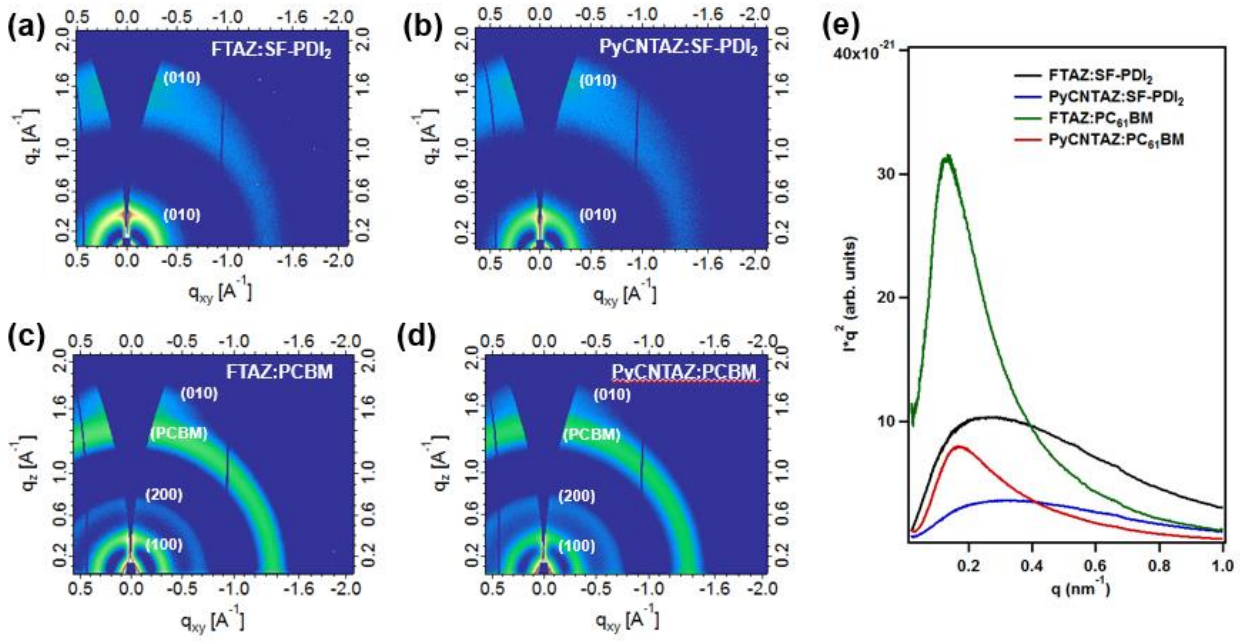

Figure 2.8 GIWAXS 2D patterns of a) FTAZ:SF-PDI$_2$, b) FTAZ:PCBM, c) PyCNTAZ:SF-PDI$_2$, and d) PyCNTAZ:PCBM blend films; e) Lorentz-corrected RSoXS profiles of the blend films

Resonant soft X-ray scattering (RSoXS) was also utilized to determine the domain spacing and relative average composition variation (ACV) of the four blend films. The Lorentz corrected RSoXS profiles acquired at a photon energy of 283.2 eV are normalized for thickness, contrast, and absorption differences (**Figure 2.8e**).[47] All RSoXS profiles are dominated by a single size distribution and the relative ACV can be extracted via integration of the scattering profiles over the full *q*-range probed and normalized to the highest ACV assigned a value of 1 (**Table 2.4**). The relative ACVs are 0.83 and 1 for FTAZ:SF-PDI_2 and FTAZ:PCBM, respectively, and 0.49 and 0.56 for PyCNTAZ:SF-PDI_2 and PyCNTAZ:PCBM, respectively. Generally, higher relative ACV (i.e., more pure domains) is important as impure domains lead to enhanced biomolecular recombination and thus lower device *FF* in both fullerene and non-fullerene based OPV systems.[48,49] In our case study, the highest relative ACV obtained in the FTAZ:PCBM film is quite consistent with its highest device *FF* up to ~73%. It is clear that the PCBM blends have more pure domains for both polymers, which is another factor contributing to the higher *FF* of the fullerene devices. The long period (domain spacing) of the SF-PDI_2 films is close to the exciton diffusion length, 25.6 nm for FTAZ:SF-PDI_2 and 20.0 nm for PyCNTAZ:SF-PDI_2. Despite having longer long period (49.0 nm for FTAZ:PCBM and 37.7 nm for PyCNTAZ:PCBM), the PCBM-based devices display higher J_{sc} and *FF* values, likely due in part to the higher charge mobility of these PCBM-based systems, which allows for more efficient charge transport and extraction. As shown in the 12%-efficiency NFA-based devices,[49,50] the blend films based on IT-M are more ordered compared with the SF-PDI_2 films. We thus speculate applying other NFAs with higher crystallinity may be a key to overcome the current limitations and further boost the efficiency of non-fullerene devices based on FTAZ and PyCNTAZ polymers.

Table 2.4 Domain characteristics of the four blend films extracted from RSoXS measurements

Blend	Domain Purity	Domain Spacing [nm]
FTAZ:SF-PDI$_2$	0.83	25.6
FTAZ:PCBM	1	49.0
PyCNTAZ:SF-PDI$_2$	0.49	20.0
PyCNTAZ:PCBM	0.56	37.7

2.3 Conclusions

Solar cells based on the non-fullerene acceptor SF-PDI$_2$ have a larger V_{oc} than those based on PCBM, however, they also have a lower J_{sc} and *FF*, leading to a decreased overall power conversion efficiency. The increased V_{oc} in the non-fullerene devices is explained by the higher-lying LUMO level of SF-PDI$_2$, which increases the $HOMO_{Donor} - LUMO_{Acceptor}$ gap, and more importantly, leads to a higher E_{CT} for these devices. In all four devices, the energy loss due to non-geminate recombination (ΔE_{NG}) is very similar (~ 0.6 eV), yet the driving force for charge separation (ΔE_{CS}) is exceptionally small (~ 0.03 eV) for the PyCNTAZ-based devices (with either PCBM or SF-PDI$_2$ as the acceptor). This interesting discovery certainly warrants further investigation. For example, what structural features of molecules would lead to such a low ΔE_{CS}? On the other hand, the SF-PDI$_2$-based devices show insufficient charge generation, transport and collections, which would explain the low J_{sc} of these devices. Notably, the light intensity dependence of V_{oc} and J_{sc} indicates more recombination loss channels, including trap-assisted recombination and surface recombination in the SF-PDI$_2$-based devices, in addition to the already increased bimolecular recombination loss in these devices. All these recombination

losses would account for the decreased J_{sc} for the SF-PDI_2-based solar cells. Finally, the SF-PDI_2-based devices demonstrate less pure domains, low electron mobilities, and an imbalance in the electron and hole mobilities, all of which contribute to the observed decrease in *FF*.

In summary, our understanding of the causes of the decreased J_{sc} and *FF* generally observed in non-fullerene acceptor based OPVs, can aid in the design of new non-fullerene acceptors with improved J_{sc} and *FF*, while maintaining the potential increase in V_{oc} in these non-fullerene acceptor based solar cells.

2.4 Experimental

2.4.1 Synthesis

FTAZ,[29] PyCNTAZ,[30] and SF-PDI_2[28] were synthesized according to literature procedure. The purity of all synthesized molecular materials were confirmed by NMR analysis.

2.4.2 Device Fabrication

Solar cells were fabricated on glass substrates with patterned indium doped tin oxide (ITO). The ITO substrates were sonicated in deionized water, acetone, and isopropyl alcohol for fifteen minutes each, followed by UV-ozone treatment for 15 minutes. For FTAZ devices, PEDOT:PSS (Clevios PH500 from Heraeus) was spun cast on the cleaned ITO at 4000 rpm for 60 s, then baked at 130°C for fifteen minutes in air. The substrates were then transferred into a nitrogen filled glovebox. For PyCNTAZ devices, CuSCN was dissolved in dipropylsulfide (20 mg/mL) and stirred for 24 h, after which the saturated solution was filtered with a 0.2 μm poly(tetrafluoroethylene) (PTFE) filter. CuSCN was spun cast onto the cleaned ITO substrated at 1000 rpm for 60 s, then baked at 80°C for 15 min in a glovebox under nitrogen atmosphere.

Donor:acceptor blend solutions were prepared (D:A=1:2, 7 mg/mL polymer for all four solutions) in 1,2,4-trichlorobenzene and stirred at 130°C for 5 h. The solutions were spun cast onto the PEDOT:PSS or CuSCN films for 60 s at the appropriate speed and then dried under vacuum to yield ~150 nm films. The devices were finished by evaporation of 30 nm of calcium and 70 nm of aluminum as the cathode and tested under AM 1.5G irradiation calibrated with an NREL certified standard silicon solar cell. Current density-voltage curves were measured via a Keithley 2400 digital source meter.

2.4.3 SCLC Measurements

Electron and hole mobilities were measured via the space-charge limited current (SCLC) method. Electron-only devices were fabricated with the configuration ITO/PEI/Donor:Acceptor/Ca/Al, where PEI is polyethyleneimine, used for reducing the work function of ITO.[51] Hole-only devices were fabricated with the configuration ITO/HTL/Donor:Acceptor/MoO_3/Al, where the HTL was PEDOT:PSS for FTAZ-based devices and CuSCN for PyCNTAZ-based devices. The dark current densities were measured with an applied voltage from 0 to 6 V using a Keithley 2400 digital source meter. The applied voltage was corrected from the voltage drop due to series and contact resistance. The Mott-Gurneys law was utilized to extract mobility values:

$$J = \frac{9}{8}\varepsilon_r\varepsilon_0\mu_h\frac{V^2}{L^3}$$

where ε_r is the dielectric constant of the tetramer, ε_0 is the permittivity of free space, μ_h is the hole mobility, V is the voltage drop across the device, and L is the thickness of the active layer.

2.4.4 Long Wavelength EQE Measurements

Devices for long wavelength EQE measurements were spun cast at University of North Carolina Chapel Hill, and the top contacts were evaporated at North Carolina State University. Active layer thicknesses were ~150 nm for both FTAZ devices and ~120 nm for PyCNTAZ devices. Long wavelength EQE measurements were conducted using an in-house setup consisting of a Xenon DC arc lamp, an ORIEL 74125 monochromator, a Keithley 428 current amplifier, an SR 540 chopper system and a Stanford Research Systems SR830 DSP lock-in amplifier. For the calibration of the spectrum, a Si and a Ge photodiode purchased from Newport Corporation were used as necessary. A 700 nm and 1000 nm long-pass filters were used in order to isolate the desired part of the spectrum for the monitoring of the sub-bandgap response.

2.4.5 Morphology

GIWAXS, R-SoXS and NEXAFS reference spectra measurements were respectively performed at the beamline 7.3.3 [52] and beamline 11.0.1.2,[53] beamline 5.3.2.2,[54] Advanced Light Source (ALS), Lawrence Berkeley National Laboratory, following the previously established protocols. GIWAXS data were acquired just above the critical angle (0.13°) of the films with a hard X-ray energy of 10 keV, and Silver Behenate (AgB) was used for geometry calibration. R-SoXS was performed in a transmission geometry with linearly polarized photons under high vacuum (1×10^{-7} torr) and a cooled (-45 °C) CCD (Princeton PI-MTE, 2048 pixels×2048 pixels) was used to capture the soft X-ray scattering 2D maps and PS300 was used for geometry calibration. The raw 2D X-ray data was processed with a modified version of NIKA into 1D scattering profiles I(q).[55]

CHAPTER 3: DONOR POLYMER FLUORINATION DOUBLES THE EFFICIENCY IN NON-FULLERENE ORGANIC PHOTOVOLTAICS[2]

3.1 Introduction

A popular and effective method to improve the power conversion efficiency (PCE) of polymer solar cells (PSCs) is fluorination of the donor polymer.[6,56–58] One successful, well-studied example of donor fluorination is the copolymer of benzodithiophene (BnDT) and fluorinated benzotriazole (FTAZ), which was introduced in 2011 by Price et al.[29] In that study, the performance of FTAZ in bulk heterojunction (BHJ) devices was compared with that of its non-fluorinated counterpart, HTAZ (**Chart 3.1**). Price et al. found that fluorination increased the short circuit current (J_{sc}), open circuit voltage (V_{oc}), and fill factor (*FF*) of the solar cells, leading to an overall improvement in PCE from 4.3% to 7.1% for HTAZ and FTAZ, respectively. Later, Li et al. optimized the molecular weight of FTAZ[31] and designed a series of BnDT-(X)TAZ polymers with varying amounts of fluorination (from 0 to 100% F) to further investigate the impact of fluorine in this system.[25] The authors found that PCE increased as amount of fluorine increased, due mainly to an increase in *FF*. Through a comprehensive study of device properties, this increase in *FF* was attributed solely to an increase in hole mobility with increased fluorination.[25]

Recently, non-fullerene acceptors (NFAs) have become more popular as electron acceptors than traditional fullerene derivatives in PSCs.[7,8,59] Compared with fullerene

[2] Reprinted with permission from Bauer, N.; Zhang, Q.; Zhu, J.; Peng, Z.; Yan, L.; Zhu, C.; Ade, H.; Zhan, X.; You, W. *J. Mater. Chem. A*, **2017**, *5*, 22536-22541

derivatives, NFAs benefit from improved light absorption and easier tuning of optoelectronic properties, allowing for complementary absorption and energy level matching with those of donor polymers to improve J_{sc} and V_{oc}. Among all NFAs, ITIC (**Chart 3.1**) and its derivatives are the most studied and have shown great potential in advancing the efficiency of polymer solar cells. ITIC has an indacenodithieno[3,2-b]thiophene core and 2-(3-oxo-2,3-dihydroinden-1-ylidene)malononitrile end groups, and was first introduced as a NFA by Lin et al. in 2015.[10] When ITIC was paired with PTB7-Th, a popular donor polymer, in BHJ solar cells, a PCE of 6.80% was obtained, which was the highest efficiency for NFA-based devices at that time. Since then, ITIC and its derivatives have become commonly used acceptor molecules to reach higher PCEs for PSCs.[14,19,68,69,60–67] Just recently, Zhao et al. found that fluorination of the acceptor molecule can also lead to improved PSC performance. They designed a fluorinated ITIC derivative which, when paired with the FTAZ polymer, achieved a PCE of 13.1%, the highest reported efficiency for PSCs to date.[70]

While there are a few reports of donor polymer fluorination improving efficiency in NFA-based solar cells,[17,71] the majority of work on the so-called "F effect" has been focused on fullerene-based systems (e.g., PCBM, Phenyl-C_{61}-butyric acid methyl ester). In this study, we aim to investigate the impact of donor polymer fluorination in these NFA-based systems, and determine if fluorination has a positive effect on device performance similar to that in fullerene-based devices. To accomplish this, we have fabricated BHJ devices with either non-fluorinated TAZ (i.e., HTAZ) or its fluorinated version (i.e., FTAZ) as the donor polymer and ITIC as the non-fullerene acceptor, as FTAZ has proven to be a good match for ITIC and its derivatives in previous reports.[60,61] By studying the photovoltaic and morphological properties of the FTAZ:ITIC and HTAZ:ITIC devices, we found that fluorination also led to an increased PCE in

this NFA-based system due in part to an improved V_{oc} and *FF*. This result is similar to these polymers with PCBM[29]; however, unlike the PCBM-based devices, the increase in efficiency for the ITIC-based devices was also in large part due to an increase in J_{sc} with fluorination.

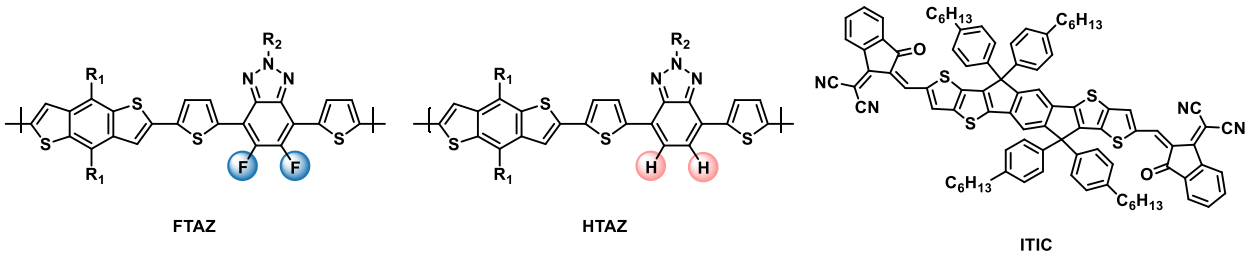

Chart 3.1 Chemical structures of FTAZ, HTAZ, and ITIC

3.2 Results and Discussion

3.2.1 Optical and Electrochemical Properties

We first considered the optical and electronic properties of FTAZ, HTAZ, and ITIC. As displayed in **Figure 3.1a**, the absorption of both FTAZ and HTAZ is complementary to that of ITIC, which would allow for an improved J_{sc} compared to fullerene-based devices with these polymers. The highest occupied molecular orbital (HOMO) levels of the materials were measured via cyclic voltammetry (**Figure B1**), and the lowest unoccupied molecular orbital (LUMO) levels were calculated using the HOMO level and absorption onset from UV-Vis spectra. The HOMO and LUMO levels of the materials are displayed in **Figure 3.1b.** As expected, the HOMO level of FTAZ is lowered compared to that of HTAZ, due to the electron-withdrawing nature of the fluorine substituents, which would lead to an increase in V_{oc} for the FTAZ-based photovoltaic devices.

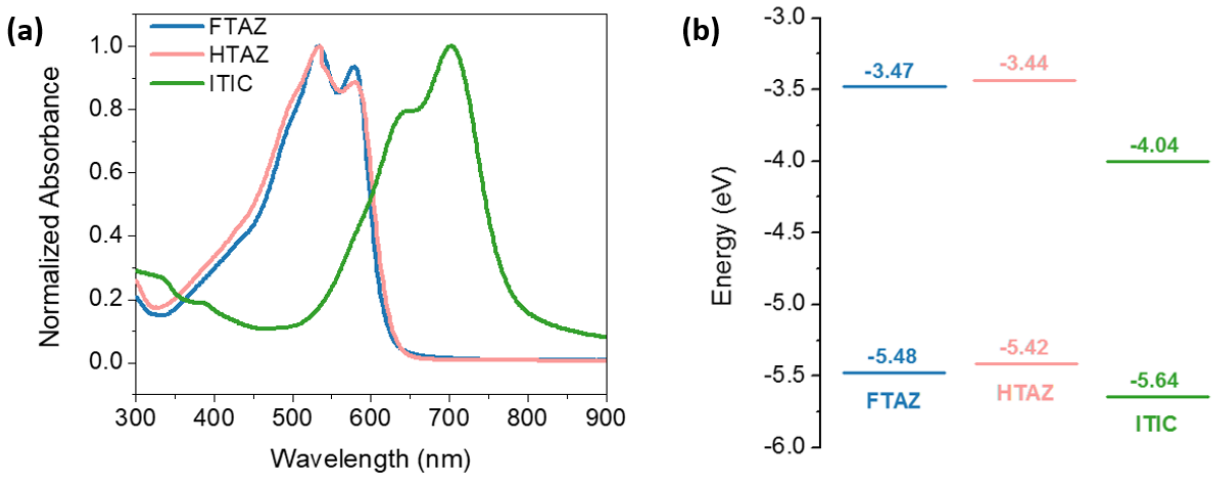

Figure 3.1 a) Normalized absorption and b) energy levels of FTAZ, HTAZ, and ITIC

3.2.2 Device Performance

To determine the effect of fluorination on photovoltaic performance, bulk heterojunction devices were prepared with a device structure of ITO/ZnO/polymer:ITIC/MoO_3/Al, a polymer:ITIC ratio of 1:1.5 and an active layer thickness of ~90 nm. The photovoltaic characteristics are given in **Table 3.1**, with representative J-V curves displayed in **Figure 3.2a**. As expected, addition of fluorine substituents led to an increase in V_{oc} due to the lower HOMO level of FTAZ, as V_{oc} is largely correlated to the difference between the HOMO level of the donor and LUMO of the acceptor. Fluorination also led to a 40% improvement in *FF*, which is similar to that observed in the fullerene-based devices for these polymers.[29] Additionally, the FTAZ:ITIC device also displayed a large increase in J_{sc}, with a J_{sc} 30% higher than that of the HTAZ:ITIC device. Notably, this improvement in J_{sc} has not been observed in previously published studies of PCBM-based devices with these TAZ polymers. Overall, the power conversion efficiency of FTAZ:ITIC (8.37%) was nearly double that of HTAZ:ITIC (4.26%), due mainly to the increase in both J_{sc} and *FF*. This efficiency of ~8% for FTAZ:ITIC is similar

to those obtained when the donor polymer FTAZ was paired with other high-performing, non-fluorinated ITIC derivatives.[60,61]

In addition to the *J-V* characteristics, the external quantum efficiency (EQE) of the devices was measured. As shown in **Figure 3.2b**, both FTAZ:ITIC and HTAZ:ITIC display a broad EQE response with contributions from both the donor and acceptor; however, FTAZ:ITIC has a higher response across the entire spectrum, reaching a maximum of ~70% compared to only ~60% for HTAZ:ITIC. This increase in EQE for FTAZ:ITIC is consistent with the improved J_{sc} observed in the FTAZ-based device.

Table 3.1 Photovoltaic characteristics of FTAZ:ITIC and HTAZ:ITIC solar cells

Blend	V_{oc} (V)	J_{sc} (mA/cm^2)	*FF* (%)	PCE (%)
FTAZ:ITIC	0.911 ± 0.001	16.25 ± 0.46	56.5 ± 1.5	8.37 ± 0.40
HTAZ:ITIC	0.851 ± 0.001	12.54 ± 0.49	39.9 ± 0.9	4.26 ± 0.24

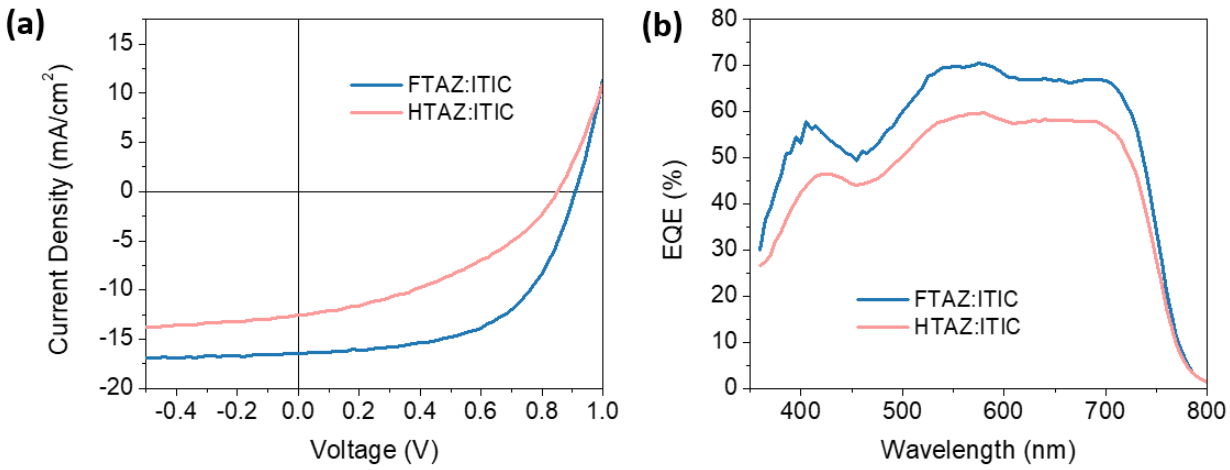

Figure 3.2 a) Representative J-V curves and b) EQE spectra of FTAZ:ITIC and HTAZ:ITIC BHJ devices

3.2.3 Device Physics

To further understand the effect of donor polymer fluorination in these devices, we first investigated the cause of the large J_{sc} increase in the FTAZ:ITIC device. We chose to focus on the increase in J_{sc} first rather than the similarly large increase in *FF*, because the J_{sc} improvement was not previously observed in PCBM-based devices with HTAZ and FTAZ. In order to understand this enhancement in J_{sc}, we needed to consider the various processes involved in current generation in PSCs. To generate current, an exciton needs to first be formed and subsequently dissociated into free charge carriers at the donor-acceptor (D-A) interface. Then, these free charge carriers need to be transported through the device and extracted at the electrodes before recombination occurs.

We first studied the exciton dissociation by measuring the photoluminescence (PL) quenching in these blends (**Figure 3.3**). As shown in **Figure 3.3a**, ITIC is able to quench the PL of both FTAZ and HTAZ nearly completely, with a similar quenching efficiency of ~99% for

both blends. Similarly, both polymers are able to efficiently quench the PL of ITIC, as displayed in **Figure 3.3b**. The high PL quenching efficiency for all materials suggests efficient exciton dissociation in both the FTAZ- and HTAZ-based devices, likely due to a morphology with small and/or mixed enough domains.

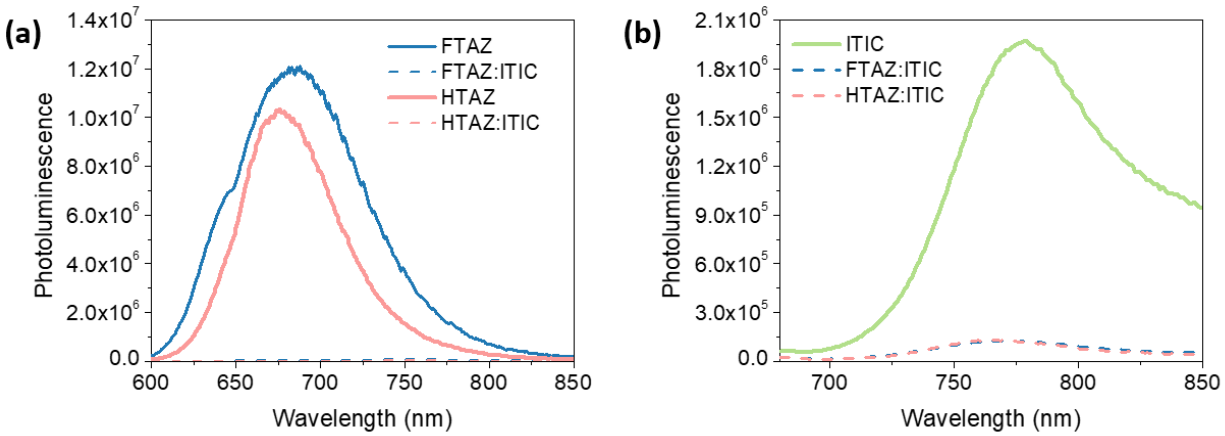

Figure 3.3 Photoluminescence of a) neat FTAZ and HTAZ (excitation at 530 nm) and b) neat ITIC (excitation at 650 nm) and both BHJ blend films

We then considered the recombination mechanisms occurring in the devices, as recombination will compete with charge extraction and lower the current generation. To gain insight into the recombination mechanisms in the FTAZ:ITIC- and HTAZ:ITIC-based devices, we measured the light intensity dependence of both J_{sc} and V_{oc} (**Figure 3.4**). J_{sc} is known to have a power law dependence on light intensity, and the slope of the J_{sc} vs intensity log plot will equal one if there is minimal bimolecular recombination in the device.[37] From the log-log plot of J_{sc} vs light intensity shown in **Figure 3.4a**, it is clear that the FTAZ:ITIC and HTAZ:ITIC devices have the same slope, indicating a similar degree of bimolecular recombination in these devices at short circuit condition. The slope for both the FTAZ- and HTAZ-based device is 0.88, which

signifies there is a small amount of bimolecular recombination for both devices. In a previous study,[72] the light intensity dependence of the FTAZ:PCBM-based device was also studied. The slope of the log-log plot was determined to be 0.93, indicating a slightly lower degree of bimolecular recombination in the PCBM-based device than the ITIC-based device studied here.

The V_{oc} dependence on light intensity is displayed in **Figure 3.4b**. When bimolecular recombination is the sole loss mechanism, a plot of V_{oc} vs the natural log of light intensity will have a slope equal to kT/q.[37] Similar to J_{sc}, the V_{oc} dependence on light intensity shows comparable slopes for both the FTAZ- and HTAZ-based device, with a slope of 0.91 kT/q and 0.85 kT/q for FTAZ:ITIC and HTAZ:ITIC, respectively. This again indicates a similar degree of recombination in these devices, which decreases the overall current generation for both blends. Additionally, these values suggest that bimolecular recombination is the dominant mechanism in these devices as opposed to monomolecular, as monomolecular recombination will lead to a slope of 2 kT/q in the V_{oc} vs intensity plot.[39] The results obtained from the light intensity study are similar to those obtained by Li et al. in their earlier study,[25] where they found that all devices had nearly identical bimolecular recombination coefficients, regardless of fluorination amount. Here, we demonstrate that replacing PCBM with ITIC as the acceptor again leads to a comparable degree of recombination in both the fluorinated (FTAZ) and non-fluorinated (HTAZ) polymer.

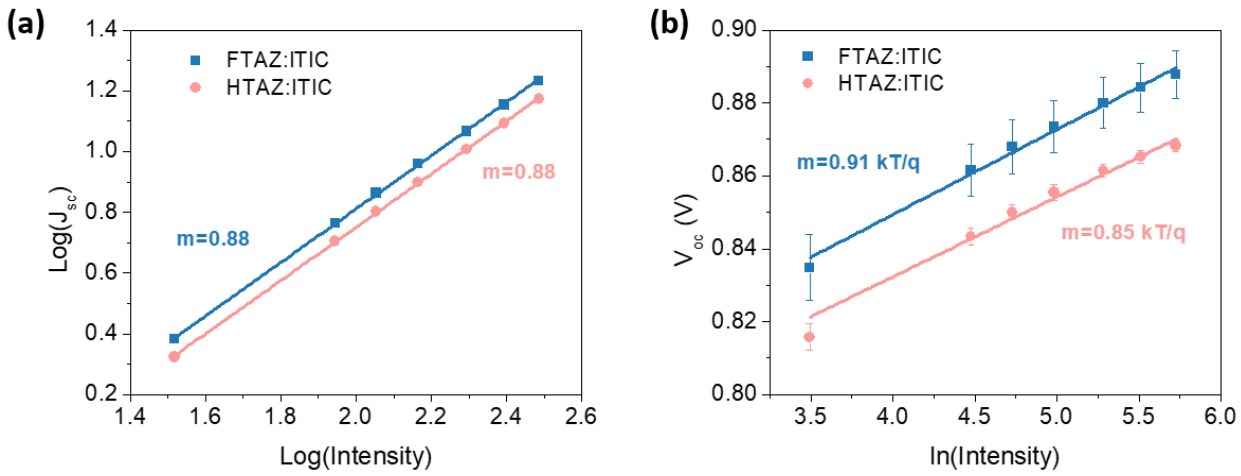

Figure 3.4 Light intensity dependence of a) J_{sc} and b) V_{oc} for the FTAZ:ITIC and HTAZ:ITIC devices

After exciton dissociation, the newly generated free charge carriers need to be transported through the device and extracted at the electrodes to generate current. To study the charge transport in these solar cells, we first measured the charge mobility via the space charge limited current (SCLC) method. The electron and hole mobility values are given in **Table 3.2**. The device based on fluorinated FTAZ displays a higher electron and hole mobility than that of the device based on non-fluorinated HTAZ. This higher charge mobility would lead to improved charge transport in the FTAZ:ITIC-based device, contributing to the improvement in J_{sc} and also in *FF*. Although the FTAZ:ITIC-based device has higher mobility values than that of the HTAZ:ITIC-based device, the mobility observed in both blends is still low, on the order of only 10^{-5} cm^2 V^{-1} s^{-1} for hole mobility and 10^{-6} for electron mobility. These low mobility values, along with the imbalance in the hole and electron mobility, could be a contributing factor to the lower fill factors observed in these devices, due to the potential for a build-up of space charge that would increase the bimolecular recombination and be detrimental to charge transport.[44]

Table 3.2 Electron and hole mobility values for the FTAZ:ITIC and HTAZ:ITIC devices

Blend	Hole Mobility ($\times 10^{-5}$ cm^2 V^{-1} s^{-1})	Electron Mobility ($\times 10^{-5}$ cm^2 V^{-1} s^{-1})
FTAZ:ITIC	9.3 ± 1.4	0.59 ± 0.17
HTAZ:ITIC	1.9 ± 0.6	0.15 ± 0.06

To further understand the charge transport and extraction in these PSCs, we measured the photocurrent and charge collection probability (**Figure 3.5**). The photocurrent (J_{ph}) is calculated by subtracting the dark current density (J_D) from the current density under illumination (J_L). This value can then be plotted against the effective voltage, V_{eff}, which is found by subtracting the applied voltage (V) from the compensation voltage (V_0) at which J_{ph} is equal to zero.[42] The plot of J_{ph} vs V_{eff} gives insight to the saturated photocurrent, $J_{ph,sat}$, which is the point at which all free carriers are extracted to the electrodes with minimal recombination. The saturated photocurrent is independent of the electric field, and affected by both field-independent losses and the optical absorption of the film.[43] **Figure 3.5a** demonstrates that the FTAZ:ITIC-base device has a higher $J_{ph,sat}$ than that of the HTAZ:ITIC-based device, which agrees with the higher J_{sc} of this device. This increase in photocurrent could be due in part to the higher absorption of the FTAZ-based blend compared to that of the HTAZ-based one (**Figure B2**). Additionally, by normalizing the photocurrent with respect to $J_{ph,sat}$, we are able to calculate the charge collection probability (P_c) of the devices (**Figure 3.5b**).[43] The FTAZ:ITIC-based device displays a higher P_c than that of the HTAZ:ITIC-based one, indicating more efficient charge extraction in the FTAZ-based device, which would lead to a higher current compared to the HTAZ-based device.

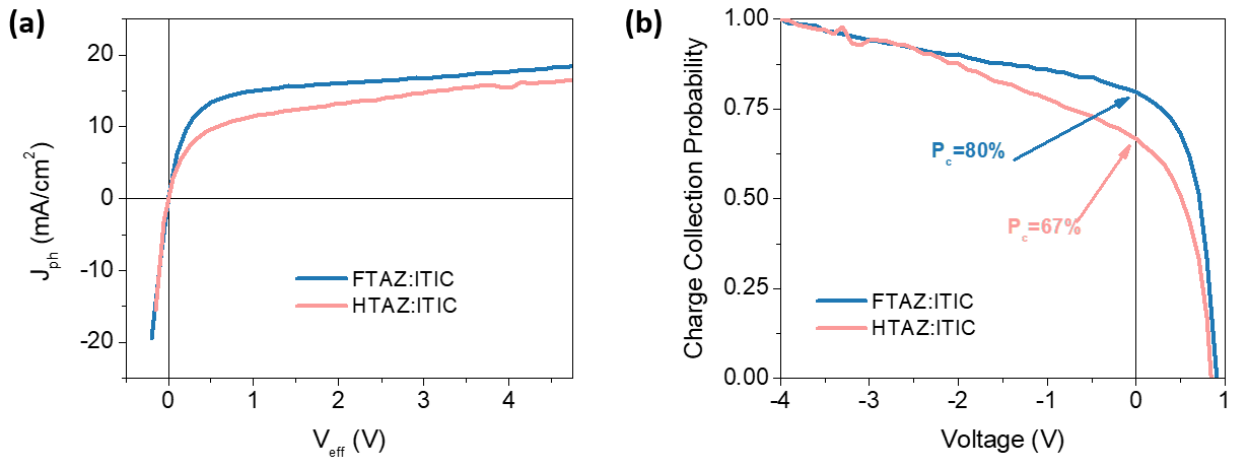

Figure 3.5 a) Photocurrent and b) charge collection probability of the FTAZ:ITIC and HTAZ:ITIC devices

3.2.4 Morphology

We also studied the morphology of the BHJ blend films, as morphology can have a large effect on photovoltaic properties. Grazing incidence wide angle X-ray scattering (GIWAXS) was used to determine the molecular packing within the film. As displayed in the 2D GIWAXS patterns for these blend films (**Figure 3.6**), both the FTAZ:ITIC blend film and the HTAZ:ITIC blend film display similar, mostly amorphous packing. The disorder in these films could play a large role in the low charge mobility values discussed previously. It is possible that improving the crystallinity in these blends would lead to improved charge transport and further increase the performance for these polymer systems. In addition to the GIWAXS data, resonant soft X-ray scattering (RSoXS) was utilized to measure the domain spacing and relative composition variations of the BHJ films. The RSoXS data have been corrected using the Lorentz correction (**Figure B6**) with the assumption of a globally isotropic 3-dimensional morphology and that long periods of Lorentz-corrected profiles give a good agreement to real-space domain spacing, which

has already been justified.[73,74] The relative composition variations, related to domain purities, are 1 and 0.9 for FTAZ:ITIC and HTAZ:ITIC, respectively (**Table 3.3**). The more pure domains for the FTAZ:ITIC blend trends with the higher *FF* observed for its device, as impure domains can lead to increased bimolecular recombination and reduce the *FF*. Additionally, the FTAZ:ITIC blend has a smaller domain spacing of 50 nm compared to 60 nm for the HTAZ:ITIC one, which is beneficial for charge transport and agrees with the higher J_{sc} for the FTAZ:ITIC-based photovoltaic device.

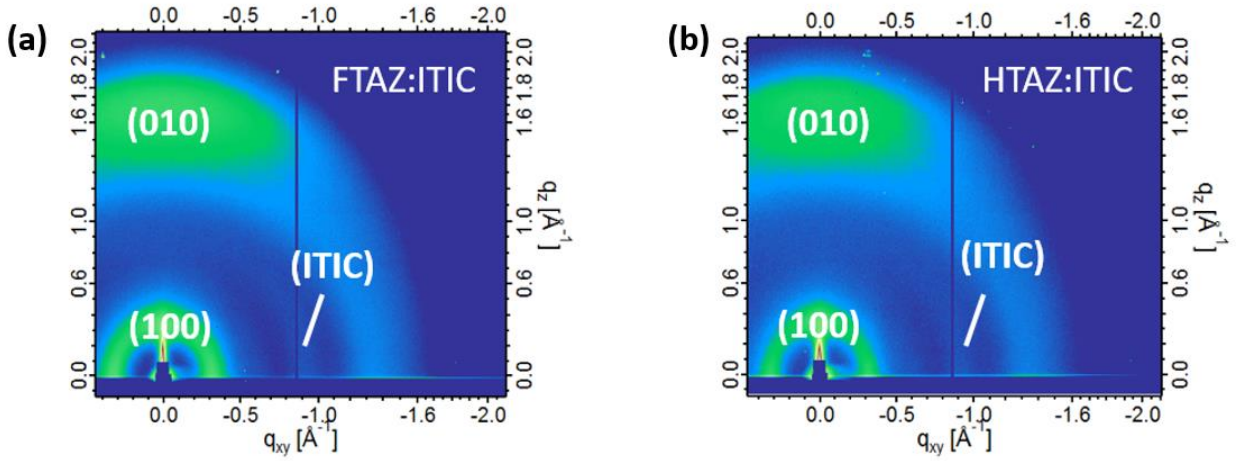

Figure 3.6 2D GIWAXS patterns for a) FTAZ:ITIC and b) HTAZ:ITIC films

Table 3.3 Domain spacing and relative purity for FTAZ:ITIC and HTAZ:ITIC blends from RSoXS data

Blend	Domain spacing (nm)	Relative Composition Variations
FTAZ:ITIC	50.2	1
HTAZ:ITIC	59.8	0.9

3.3 Conclusions

In summary, with FTAZ/HTAZ as the exemplary conjugated polymers, we show that fluorination of the donor polymer also leads to much improved device performance in solar cells with ITIC as the non-fullerene acceptor, similar to our previous discovery of fluorination-induced-efficiency enhancement in fullerene (e.g., PCBM)-based devices. The observed increase in V_{oc} with fluorination – in both PCBM-based devices and ITIC-based ones – can be ascribed to the lower HOMO level of the fluorinated FTAZ compared to its non-fluorinated counterpart HTAZ. Furthermore, the increase of *FF* by 40% from HTAZ to FTAZ in their ITIC-based devices – also similar to the *FF* enhancement observed in their PCBM-based devices – can be largely explained by the increased hole mobility with fluorination, as well as the increase in electron mobility. However, a large improvement of 30% was observed for the J_{sc}, which was not seen in previous studies of these two polymers in their PCBM-based BHJ solar cells. By studying the various processes involved in current generation in PSCs, we determined that the increase in J_{sc} for the ITIC-based devices is due to improved charge transport and extraction in the FTAZ:ITIC-based device compared to HTAZ:ITIC-based one, stemming from the higher

electron and hole mobility, as well as a higher saturated photocurrent and charge collection probability for the FTAZ:ITIC-based device.

The results of this study demonstrate that donor polymer fluorination is also a viable method to further increase efficiency in NFA-based PSCs, and may improve performance through different mechanisms than those observed in fullerene-based PSCs. To fully understand the "F effect" in NFA-based solar cells, further study is required utilizing other efficient, fluorinated donor polymers, such as those recently reported by Zhang et al.[75] Additionally, there have been a few reports demonstrating that fluorination of the non-fullerene acceptor leads to improved device performance[61,70], which should also be considered in future studies of the "F effect."

3.4 Experimental

3.4.1 Device Fabrication

Solar cells were fabricated on glass substrates with patterned indium doped tin oxide (ITO). ITO substrates were cleaned via sonication in deionized water, acetone and isopropyl alcohol for fifteen minutes each, followed by UV-ozone treatment for 15 minutes. The ZnO precursor solution was prepared by dissolving 1 g zinc acetate dihydrate and 0.28 g ethanolamine in 10 mL of 2-methoxyethanol. The solution was stirred overnight, and then spun cast onto the cleaned ITO at 6000 rpm for 60 s, then baked at 200°C for 30 minutes in air. The substrates were then transferred into a nitrogen filled glovebox. Polymer:ITIC solutions (D:A=1:1.5, 6 mg/mL polymer) in chloroform were prepared for both polymers and spun cast at 5000 rpm for 60 s. The solar cells were finished by evaporation of 10 nm MoO_3 and 50 nm of aluminum, with a device area of 13 mm^2, and tested under AM 1.5G irradiation calibrated with an NREL certified

standard silicon solar cell. Current density-voltage curves were measured via a Keithley 2400 digital source meter.

3.4.2 SCLC Measurements

Electron and hole mobilities were measured via the space-charge limited current (SCLC) method. Electron-only devices were fabricated with the configuration ITO/ZnO/Polymer:ITIC/Ca/Al, and hole-only devices were also prepared with the configuration ITO/PEDOT:PSS/Polymer:ITIC/MoO_3/Al. The dark current densities were measured with an applied voltage from 0 to 6 V using a Keithley 2400 digital source meter. The applied voltage was corrected from the voltage drop due to series and contact resistance. The Mott-Gurneys law was utilized to extract mobility values:

$$J = \frac{9}{8}\varepsilon_r \varepsilon_0 \mu_h \frac{V^2}{L^3}$$

where ε_r is the dielectric constant of the tetramer, ε_0 is the permittivity of free space, μ_h is the hole mobility, V is the voltage drop across the device, and L is the thickness of the active layer.

3.4.3 Morphology

GIWAXS, R-SoXS and NEXAFS reference spectra measurements were respectively performed at the beamline 7.3.3[52] and beamline 11.0.1.2,[53] beamline 5.3.2.2,[54] Advanced Light Source (ALS), Lawrence Berkeley National Laboratory, following the previously established protocols. GIWAXS data were acquired just above the critical angle (0.13°) of the films with a hard X-ray energy of 10 keV, and Silver Behenate (AgB) was used for geometry calibration. R-

SoXS was performed in a transmission geometry with linearly polarized photons under high vacuum (1×10^{-7} torr) and a cooled (-45 °C) CCD (Princeton PI-MTE, 2048 pixels×2048 pixels) was used to capture the soft X-ray scattering 2D maps and PS300 was used for geometry calibration. The raw 2D X-ray data was processed with a modified version of NIKA into 1D scattering profiles I(q).[55]

CHAPTER 4: THE IMPACT OF FLUORINATION ON BOTH DONOR POLYMER AND NON-FULLERENE ACCEPTOR: THE MORE FLUORINE, THE MERRIER[3]

4.1 Introduction

Fluorination of the donor polymer is an effective, well-studied method to improve the power conversion efficiency (PCE) of organic photovoltaics (OPVs).[6,76–78] By adding fluorine substituents to the donor polymer, both the HOMO and LUMO levels are pulled down simultaneously, increasing the open-circuit voltage (V_{oc}) without decreasing the band gap and the short-circuit current (J_{sc}).[79–82] Additionally, the small size of the fluorine atom allows for the tuning of these properties without introducing a large amount of steric hindrance to the polymer, largely maintaining the backbone planarity (and the band gap). In fact, fluorine substituents, when properly positioned, can even enhance the backbone planarity via fluorine induced non-covalent interactions.[83]

This fluorine impact continues to be studied today, in both fullerene and non-fullerene systems.[84–93] For example, Zhang et al. investigated the impact of fluorinating the thiophene linker groups in a copolymer containing benzodithiophene (BnDT) and benzotriazole (TAZ).[83] They found that fluorinating the thiophene linkers between the BnDT and TAZ moieties can lead to a similar performance as fluorinating only the TAZ unit when the polymers are paired with PCBM, and fluorinating both the thiophene and TAZ unit simultaneously can improve device

[3] Reprinted with permission from Bauer, N.; Zhang, Q.; Rech, J.; Dai, S.; Peng, Z.; Ade, H.; Wang, J.; Zhan, X.; You, W. *Nano Res*, **2019**, https://doi.org/10.1007/s12274-019-2362-3

performance. In a non-fullerene system with the small molecule acceptor IDIC, Yang et. al. compared wide band gap copolymers of quinoxaline and phenylene with varying amounts of fluorination on the phenylene unit.[94] They found that by adding up to two fluorine atoms to the phenlyene unit, the V_{oc} and J_{sc} are increased relative to having zero or one fluorine, leading to an improvement in the PCE.

Recently, non-fullerene acceptors (NFAs) have become increasingly common as a replacement for traditional fullerene derivatives, and there have been a few reports of fluorinated acceptors which outperform their non-fluorinated counterparts, similar to the donor polymers discussed previously.[95–101] For example, Zhao et al. synthesized the fluorinated acceptor ITIC-Th1, which has an indacenodithieno[3,2-*b*]thiophene (IDTT) core and fluorinated 1,1-dicyanomethylene-3-indanone (INCN) end groups.[61] The ITIC-Th1-based device exhibits a PCE of 12.1%, much higher than the 8.8% obtained by the non-fluorinated ITIC-Th. Additionally, some of the highest performing devices currently reported utilize both a fluorinated donor polymer and a fluorinated NFA.[102,103] This demonstrates that acceptor fluorination is also a promising technique to further improve the performance of OPVs.

Although NFA fluorination has been shown to increase device efficiency, there have not been many studies into the underlying causes for this improvement. Additionally, it is not yet well understood how fluorinating both the donor and NFA simultaneously impacts device performance. For future acceptor design, it is important to understand these structure-property relationships and how fluorination impacts device performance. In this study, we aim to gain a deeper understanding of why NFA fluorination leads to an improvement in device efficiency, and whether the underlying causes for this improvement are similar to those observed with donor polymer fluorination. Additionally, we will investigate how the degree of fluorination in a bulk

heterojunction (BHJ) blend impacts the device performance, and whether or not the efficiency continues to increase as fluorine is added to both the donor and acceptor.

To accomplish this, we fabricated BHJ devices with varying amounts of fluorine by using two donor polymers with either two (4'-FT-HTAZ) or four (4'-FT-FTAZ) fluorine atoms per repeat unit and two NFAs with either zero (ITIC-Th) or two (ITIC-Th1) fluorine atoms per molecule (**Chart 4.1**). We found that for each polymer, fluorination of the NFA leads to an increase in the J_{sc} and fill factor (*FF*), but a decrease in the V_{oc}. For each NFA, increasing the amount of fluorine on the donor polymer increases the V_{oc} while maintaining the J_{sc} and *FF*. The device containing the most fluorine achieved the highest PCE of over 10%, due to obtaining both a high J_{sc} and V_{oc} simultaneously.

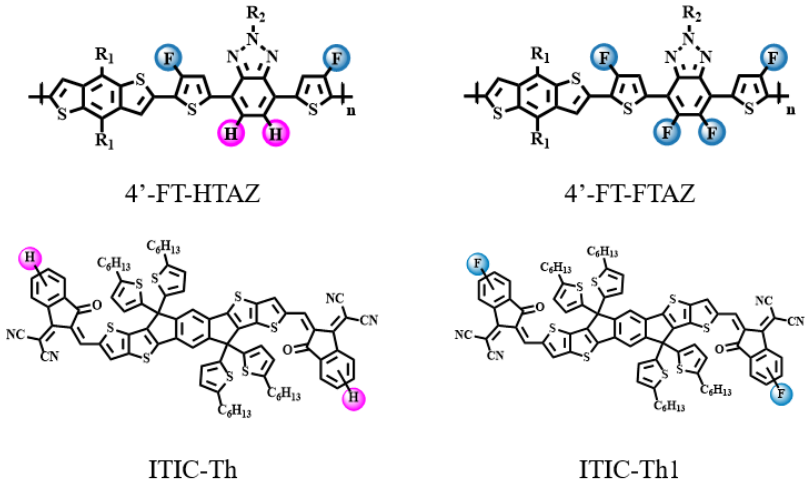

Chart 4.1 Chemical structures of 4'-FT-HTAZ, 4'-FT-FTAZ, ITIC-Th and ITIC-Th1

4.2 Experimental

4.2.1 Synthesis

4'-FT-HTAZ, 4'-FT-FTAZ,[83] ITIC-Th, and ITIC-Th1[61] were synthesized according to literature procedure.

4.2.2 UV-Vis Spectroscopy

UV-Visible absorption spectra were obtained with a Shimadzu UV-2600 spectrophotometer. Neat films were fabricated by spincasting a 15 mg/mL solution of polymer or NFA in toluene on glass. Blend films were spun cast from a 6 mg/mL polymer (D:A=1:1) solution in toluene.

4.2.3 Device Fabrication and Testing

Solar cells were fabricated on glass substrates with patterned indium doped tin oxide (ITO). ITO substrates were sonicated for fifteen minutes each in deionized water, acetone, and isopropyl alcohol, followed by UV-ozone treatment for fifteen minutes. The ZnO precursor solution was prepared by dissolving 1 g zinc acetate dihydrate and 0.28 g ethanolamine in 10 mL of 2-methoxyethanol. The solution was stirred overnight, then spun cast onto the cleaned ITO slides at 4000 rpm for 30 s and baked for 30 minutes at 150 °C in air. The substrates were then transferred to a nitrogen filled glovebox for active layer deposition. Active layer solutions (D:A=1:1, 6 mg/mL polymer) were prepared for all four blends in toluene and stirred overnight, then spun cast onto the ZnO to yield ~100 nm films. The devices were finished by evaporation of 10 nm of MoO_3 and 70 nm of aluminum to give a device area of 0.13 cm^2, then tested under AM 1.5G irradiation with an intensity of 100 mW/cm^2 (Oriel 91160, 300 W) calibrated with an

NREL certified standard silicon solar cell. Current density versus voltage (*J*-*V*) curves were recorded with a Keithley 2400 digital source meter. EQE were detected under monochromatic illumination (OrielCornerstone 260 1/4 m monochromator equipped with Oriel 70613NS QTH lamp), and the calibration of the incident light was performed with a monocrystalline silicon diode (Model No.: Newport 71580).

4.2.4 SCLC Measurements

Electron and hole mobilities were measured via the space-charge limited current (SCLC) method. Electron-only devices were fabricated with the configuration ITO/ZnO/D:A/Ca/Al, and hole-only devices were also prepared with the configuration ITO/PEDOT:PSS/D:A/MoO_3/Al. The dark current densities were measured with an applied voltage from 0 to 6 V using a Keithley 2400 digital source meter. The applied voltage was corrected from the voltage drop due to series and contact resistance. The Mott-Gurneys law was utilized to extract mobility values:

$$J = \frac{9}{8}\varepsilon_r\varepsilon_0\mu_h\frac{V^2}{L^3}$$

where ε_r is the dielectric constant of the polymer, ε_0 is the permittivity of free space, μ_h is the hole mobility, V is the voltage drop across the device, and L is the thickness of the active layer.

4.2.5 Morphology

GIWAXS, RSoXS and NEXAFS reference spectra measurements were respectively performed at the beamline 7.3.3[52] and beamline 11.0.1.2,[53] beamline 5.3.2.2,[54] Advanced Light Source (ALS), Lawrence Berkeley National Laboratory, following the previously established protocols. GIWAXS data were acquired just above the critical angle (0.13°) of the films with a hard X-ray energy of 10 keV, and Silver Behenate (AgB) was used for geometry calibration. RSoXS was performed in a transmission geometry with linearly polarized photons under high vacuum (1×10^{-7} torr) and a cooled (-45 °C) CCD (Princeton PI-MTE, 2048 pixels×2048 pixels) was used to capture the soft X-ray scattering 2D maps and PS300 was used for geometry calibration. The raw 2D X-ray data was processed with a modified version of NIKA into 1D scattering profiles I(q).[55]

4.3 Results and Discussion

4.3.1 Optical and Electrochemical Properties

We first investigated the optical and electronic properties of the donor polymers and NFAs used in this study. The absorbance spectra of the neat materials in thin film were measured by UV-Vis spectroscopy, and the results are displayed in **Figure 4.1a**. The donor polymers (4'-FT-HTAZ and 4'-FT-FTAZ) have similar absorption spectra, which are complementary to the absorption of both ITIC-Th and ITIC-Th1. Combined together, any donor/acceptor pair in this study has sufficient spectral coverage from 400 nm to 800 nm, which is beneficial for current generation in a photovoltaic device. Additionally, ITIC-Th1 displays a red-shift relative to ITIC-Th, which could lead to higher J_{sc} in a device. The HOMO levels of the donors and acceptors were measured by cyclic voltammetry, and the LUMO levels were calculated from the HOMO

levels and absorption onsets from UV-Vis (**Figure 4.1b**). As shown in **Figure 4.1b**, the energy levels of both donor polymers are well-matched with those of the two acceptors, a prerequisite to forming efficient BHJ solar cells.

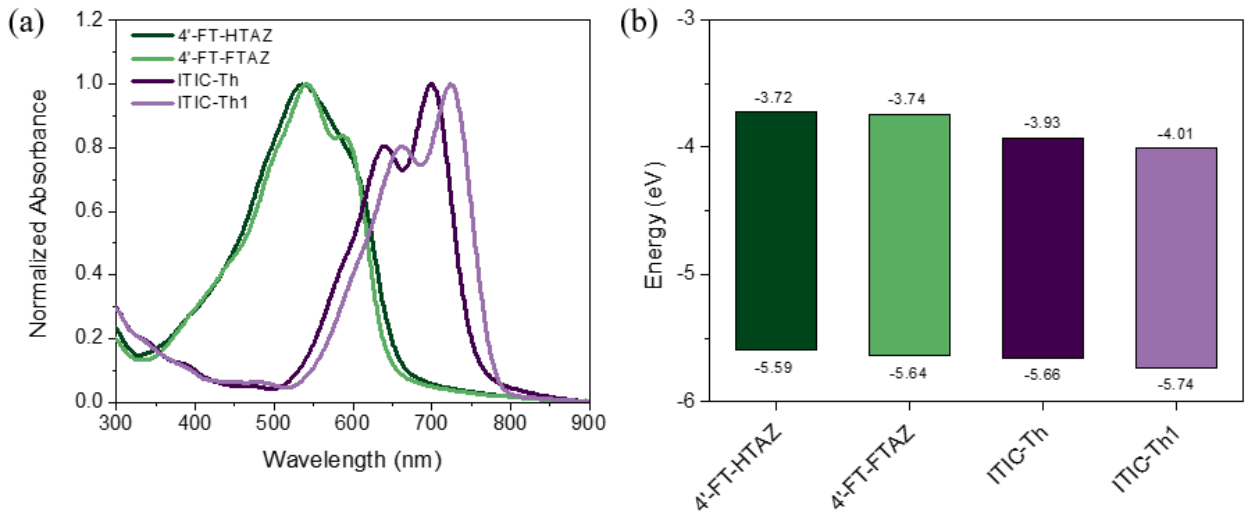

Figure 4.1 a) Normalized absorbance in thin film and b) energy levels for 4'-FT-HTAZ, 4'-FT-FTAZ, ITIC-Th, and ITIC-Th1

4.3.2 Photovoltaic Performance

We then studied the photovoltaic properties of these materials by fabricating BHJ solar cells with an inverted architecture of ITO/ZnO/Donor:Acceptor/MoO_3/Al. A summary of the results is displayed in **Table 4.1**, with representative current density-voltage (*J*-*V*) curves for each blend shown in **Figure 4.2a**. For each donor polymer, fluorinating the acceptor (i.e., from ITIC-Th to ITIC-Th1) leads to an increase in the J_{sc} and *FF*, but a decrease in the V_{oc}. This V_{oc} decrease can be ascribed to the lowered LUMO level of the fluorinated ITIC-Th1, as the difference in the LUMO levels between ITIC-Th and ITIC-Th1 (~ 0.08 eV) is approximately equal to the observed decreases in V_{oc} (for 4'-FT-HTAZ, 0.914 V – 0.851 V ≈ 0.06 V; and for 4'-

FT-FTAZ, 1.007 V – 0.924 V ≈ 0.08 V). When considering each NFA, adding more fluorine to the donor polymer (i.e., from 4'-FT-HTAZ to 4'-FT-FTAZ) leads to a quite significant increase in the V_{oc} due to the lowered HOMO level of the 4'-FT-FTAZ. For example, in the case of ITIC-Th, switching from 4'-FT-HTAZ (2F) to the further fluorinated 4'FT-FTAZ (4F), the V_{oc} of the BHJ device is increased by ~ 0.1 V (from 0.914 V to 1.007 V). ITIC-Th1-based devices also observe a 0.07 V boost in V_{oc} when switching to 4'FT-FTAZ (from 0.851 V to 0.924 V). However, there is not any major change in the J_{sc} or *FF* in the case of ITIC-Th based devices when switching from 4'-FT-HTAZ to 4'-FT-FTAZ, yet the J_{sc} for the ITIC-Th1 based devices is noticeably increased (from 4'-FT-HTAZ to 4'-FT-FTAZ). Overall, the acceptor fluorination allows for a high J_{sc} and FF, while the extra fluorination of the donor polymer recovers some of the V_{oc} loss from the lower LUMO level of ITIC-Th1, allowing for a high J_{sc} and V_{oc} simultaneously. Thus, the blend with the most fluorine, 4'-FT-FTAZ:ITIC-Th1, displays the highest overall efficiency, with an average PCE of 10.3%.

To understand the J_{sc} increase observed with acceptor fluorination, we measured the external quantum efficiency (EQE) of the devices (**Figure 4.2b**), as well as the absorption of the blend films (**Figure C2** in SI). As shown in **Figure 4.2b**, all four blends have a broad EQE response, and the responses generally match the trend in J_{sc} observed for these devices. For example, the device with the lowest current, 4'-FT-FTAZ:ITIC-Th, also displays the lowest EQE response, while the devices with higher J_{sc} values display higher responses. Additionally, it is clear that fluorination of the acceptor (i.e., from ITIC-Th to ITIC-Th1) leads to a broadening of the EQE response, as the devices based on ITIC-Th1 have a more red-shifted onset. The wider and higher EQE response corresponds well with the higher current measured for the ITIC-Th1-based devices. The conclusions that can be drawn from the absorption of the blend films (**Figure**

C2 in SI) agree with those from the EQE measurement. For each donor polymer, the blend films based on the fluorinated ITIC-Th1 display a red-shifted absorption onset compared to those based on non-fluorinated ITIC-Th. Similar to the EQE, the broader absorption of the films based on ITIC-Th1 can lead to more light absorption than for those based on ITIC-Th, which can contribute to a higher current in the device. These trends in J_{sc} and V_{oc} with acceptor fluorination (i.e. lower V_{oc} due to lowered LUMO level and higher J_{sc} due to broadened absorption) have also been reported in other systems utilizing fluorinated NFAs.[104]

Table 4.1 Photovoltaic characteristics for all four blends

Donor	Acceptor	J_{sc} (mA/cm^2)	V_{oc} (V)	FF (%)	PCE (%)
4'-FT-HTAZ	ITIC-Th	16.04 ± 0.47	0.914 ± 0.002	58.1 ± 1.3	8.53 ± 0.38
	ITIC-Th1	17.13 ± 0.65	0.851 ± 0.002	60.4 ± 1.4	8.81 ± 0.35
4'-FT-FTAZ	ITIC-Th	15.94 ± 0.48	1.007 ± 0.001	57.2 ± 1.0	9.18 ± 0.36
	ITIC-Th1	18.26 ± 1.06	0.924 ± 0.003	60.8 ± 2.6	10.27 ± 0.87

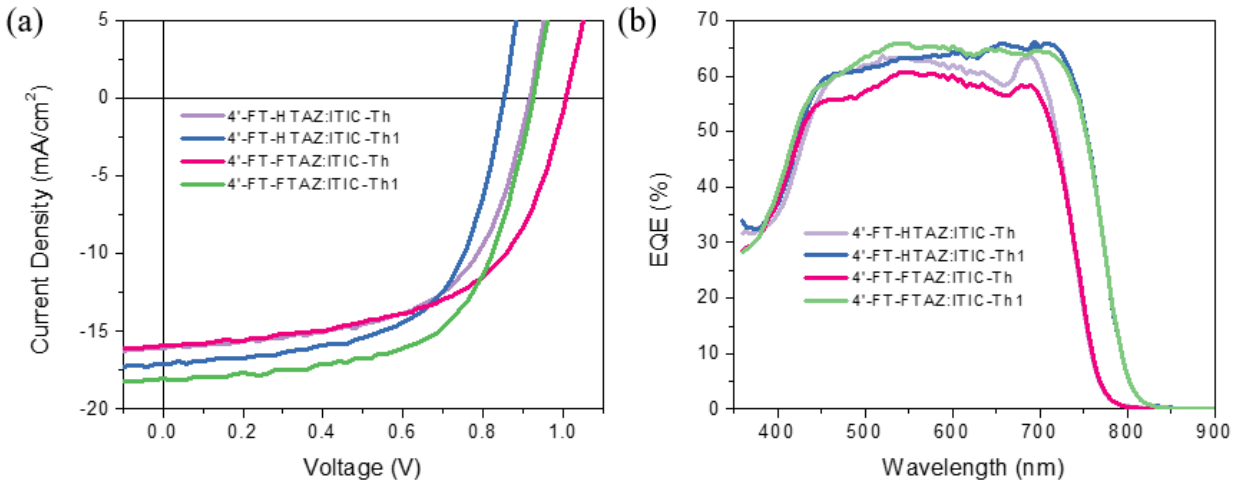

Figure 4.2 a) Representative J-V curves and b) external quantum efficiencies for all four devices

4.3.4 Light Intensity Dependence of J_{sc} and V_{oc}

In addition to light absorption, charge recombination can have a major effect on the J_{sc} as well as the *FF*.[105] To investigate whether the varying amounts of fluorination lead to differences in recombination, we measured the light intensity dependence of the J_{sc} and V_{oc} (**Figure 4.3**). **Figure 4.3a** displays a log-log plot of the J_{sc} vs intensity, and it is clear that all four blends have a similar slope of ~1, which indicates there is minimal bimolecular recombination at the short-circuit condition.[39] For the V_{oc} dependence (**Figure 4.3b**), all four blends again have a similar slope, with a value of ~1 kT/q. This slope of ~kT/q indicates that there is mainly bimolecular recombination occurring at the open-circuit condition, rather than a combination of bimolecular and monomolecular.[39] As mentioned, for both the J_{sc} and V_{oc}, the dependence on light intensity is very similar for all four blends, as evidenced by their nearly identical slopes. This suggests that the recombination is also similar in all four blends, and the amount of fluorination does not seem to play a large role in determining the recombination mechanisms.

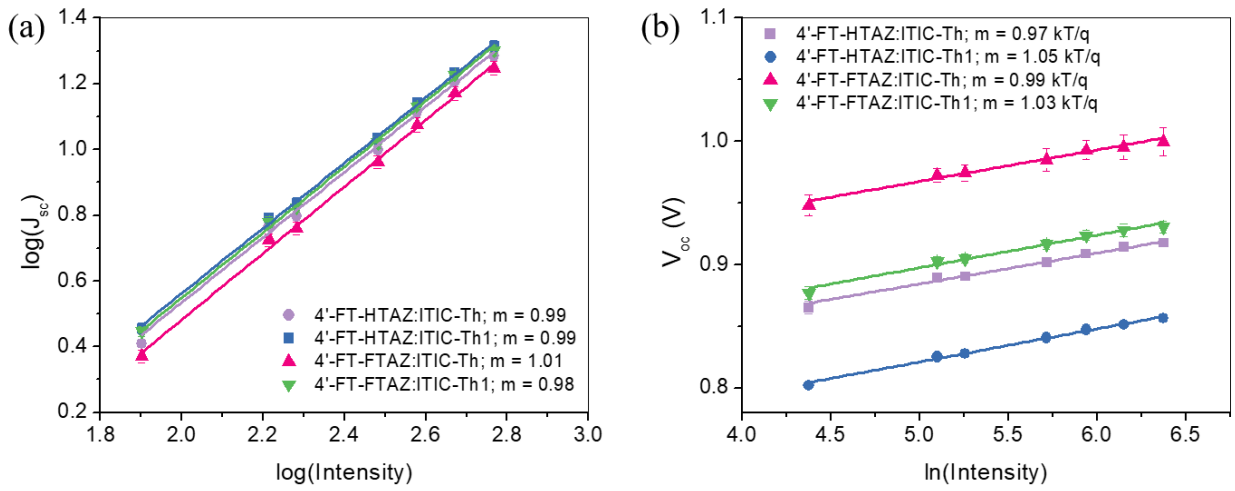

Figure 4.3 a) J_{sc} and b) V_{oc} dependence on light intensity for all four devices

4.3.5 Mobility

The charge transport and mobility is also an important factor in determining the J_{sc} and *FF* for a device; in general, higher and more balanced mobility values would lead to high *FF*.[44,106–109] To measure the hole and electron mobility of the blend films, we fabricated hole-only and electron-only devices with the structure ITO/PEDOT:PSS/D:A/MoO_3/Al and ITO/ZnO/D:A/Ca/Al, respectively. The measured mobility values, as well as the ratio of the hole to electron mobility for each blend, are shown in **Table 4.2**. For the devices based on 4'-FT-HTAZ, fluorination of the acceptor (i.e., from ITIC-Th to ITIC-Th1) leads to higher, more balanced electron and hole mobility values. On the other hand, the devices based on 4'-FT-FTAZ show an increase in electron mobility with acceptor fluorination, as well as more balanced mobility values. This agrees well with the observed trends in photovoltaic characteristics for these devices, as higher, more balanced mobility values can lead to an increase in J_{sc} and *FF*.[44,110] For each acceptor, additional fluorination of the donor polymer (i.e., from 4'-FT-HTAZ to 4'-FT-FTAZ) leads to an increase in both the hole and electron mobility values, however, the

change in μ_h/μ_e is not as drastic as it is when comparing the ITIC-Th- and ITIC-Th1-based devices with the same donor polymer. This also agrees with the observed photovoltaic performance, as the devices based on 4'-FT-FTAZ did not show a large improvement in either the J_{sc} or *FF* when compared to those based on 4'-FT-HTAZ.

Table 4.2 Hole and electron mobility values for all four blends

Donor	Acceptor	Hole Mobility ($\times 10^{-4}$ cm^2 V^{-1} s^{-1})	Electron Mobility ($\times 10^{-4}$ cm^2 V^{-1} s^{-1})	μ_h/μ_e
4'-FT-HTAZ	ITIC-Th	6.59 ± 3.26	0.0624 ± 0.0154	106
	ITIC-Th1	12.6 ± 6.11	0.262 ± 0.512	48
4'-FT-FTAZ	ITIC-Th	40.4 ± 13.1	0.294 ± 0.526	137
	ITIC-Th1	30.9 ± 11.3	1.92 ± 0.421	16

4.3.6 Morphology

We also studied the morphology of the four blend films, as it can have a large effect on device performance. Grazing Incidence Wide Angle X-ray Scattering (GIWAXS) was used to investigate the molecular packing and ordering within the films, and the results are shown in **Figure 4.4**. All four blend films show a lamellar packing peak at ~0.35 Å^{-1} in the in-plane direction and a π-π stacking peak at ~1.8 Å^{-1} in the out-of-plane direction, indicating preferential face-on orientation with respect to the substrate. From these results, it becomes clear that the amount of fluorination in the blend (on either the donor or acceptor) does not have much of an effect on the molecular packing and crystallinity, as these are very similar for all four blends. In addition to GIWAXS, resonant soft X-ray scattering (RSoXS) was used to study the domain spacing and relative root-mean-square composition variation. The data is shown in **Table 4.3**,

and the Lorentz-corrected RSoXS profiles are shown in **Figure C4**. The relative root-mean-square composition variation differs between the blends, with the fluorinated ITIC-Th1-based blends having a higher relative root-mean-square composition variation than those based on the non-fluorinated ITIC-Th. This agrees well with the observed trend in *FF*, as blends with higher relative root-mean-square composition variation usually display a higher *FF* in photovoltaic devices.[111] It should also be noted that the ITIC-Th-based blends show stronger (010) scattering peaks from the GIWAXS data, which generally corresponds to better charge transport. However, the ITIC-Th-based devices display a lower J_{sc} than those based on ITIC-Th1, which may be ascribed to their larger domain spacing indicated by the RSoXS measurements.

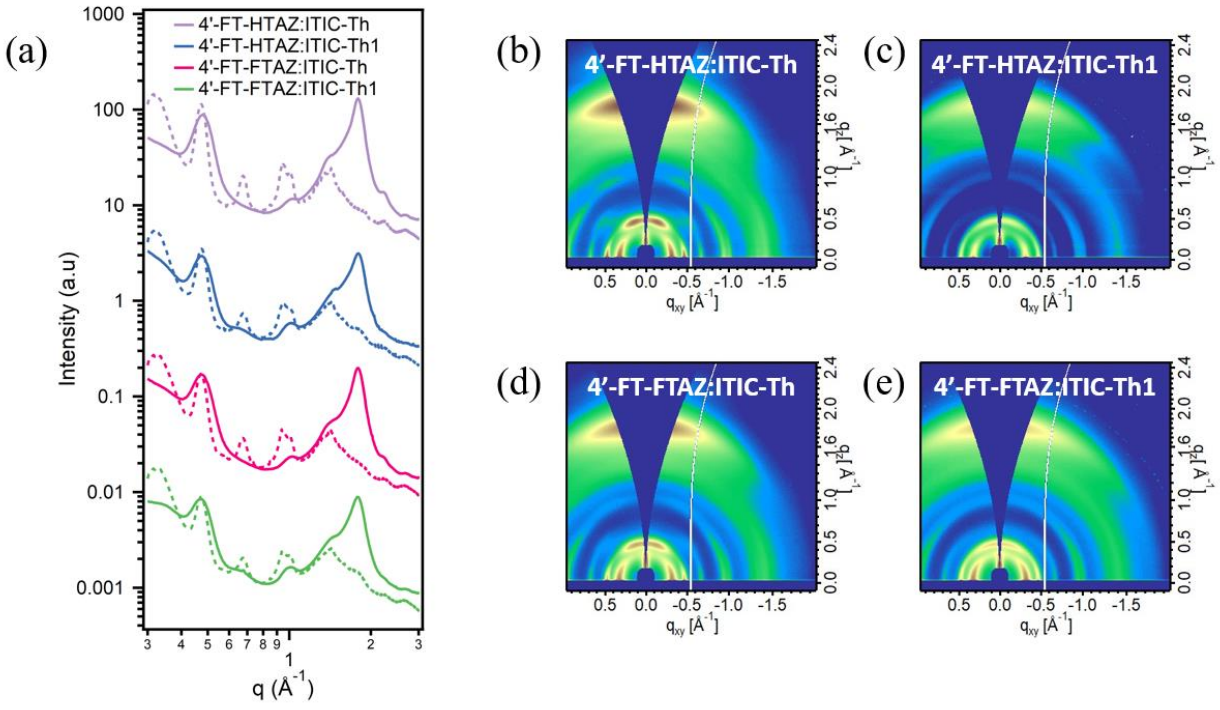

Figure 4.4 a) Sector averaged (±10°) profiles (solid line: out-of-plane direction; dotted line: in-plane direction) and b)-e) 2D GIWAXS patterns for all four blend films

Table 4.3 Domain spacing and relative root-mean-square composition variation of all four blends from RSoXS

Donor	Acceptor	Domain Spacing (nm)	Relative root-mean-square composition variation
4'-FT-HTAZ	ITIC-Th	32.54	0.543
	ITIC-Th1	31.56	0.845
4'-FT-FTAZ	ITIC-Th	30.63	0.677
	ITIC-Th1	29.76	1.000

4.4 Conclusion

In summary, using two donor polymers and two NFAs with varying amounts of fluorination (from 2F to 6F), we demonstrate and explain how a higher degree of fluorination in an active layer blend leads to an improved device performance. Fluorination of the NFA (i.e., from ITIC-Th to ITIC-Th1) extends the absorption range, leads to higher, more balanced mobility values, and increases the relative root-mean-square composition variation; all these lead to a higher J_{sc} and *FF* for the ITIC-Th1-based devices. Additional fluorination of the donor polymer also leads to an increase in electron and hole mobility values, as well as a decrease in the HOMO level of the polymer, leading to an improved V_{oc} for the devices based on 4'-FT-FTAZ when compared with those based on 4'-FT-HTAZ. Therefore, the blend with the highest number of fluorine substituents (6F), 4'-FT-FTAZ:ITIC-Th1, displayed the highest overall performance. Although showing the highest overall PCE, the 4'-FT-FTAZ:ITIC-Th1 device displays a lower V_{oc} than that based on 4'-FT-FTAZ:ITIC-Th, due to the lower LUMO level of

the ITIC-Th1. This observation indicates that, despite the large improvements in PCE obtained with the introduction of NFAs, there is still a trade-off between the J_{sc} and V_{oc}, which has been generally observed in systems containing fullerene-based acceptors.[112]

This study demonstrates that fluorination of both the donor polymer and non-fullerene acceptor is a viable method to improve device performance, and explores the fundamental reasons behind this improvement. In the design of future NFAs, fluorination should be considered as a method to improve charge mobility and increase absorption range. Additionally, fluorinated NFAs can be paired with fluorinated donor polymers, as this can lead to an improved performance when compared to solely fluorinating either the donor or the acceptor.

CHAPTER 5: CONCLUSION

5.1 Perspective

As the demand for clean, renewable energy increases, research into alternative technologies for solar energy has increased as well. Organic photovoltaics have emerged as a practical alternative to silicon due to their lower cost and ability to be easily processed from solution, allowing for large-scale roll-to-roll printing of devices. Previously, research efforts in OPVs were focused on the development of new conjugated polymer electron donors that could be paired with the electron acceptor PCBM. Recently, however, there has been a rise in the development of new, non-fullerene acceptors that have stronger light absorption and more structural versatility than PCBM. The development of NFAs has led to a dramatic increase in the efficiency of OPVs, recently reaching over 15%.[11] Despite these impressive improvements, the design criteria to obtain high-performing NFA-based OPVs is not well understood, and further study is required to better understand the requirements for even higher efficiency materials. This dissertation was focused on the investigation of a variety of NFAs to determine their structure-property relationships and better understand how the design of both the NFA and donor polymer impacts the device performance, and what features are necessary to achieve high efficiencies.

5.2 Requirements for High Performance NFAs

In Chapter 2, we directly compared the performance of the non-fullerene acceptor SF-PDI_2 to that of PCBM by fabricating solar cells using the two acceptors and two donor polymers (FTAZ and PyCNTAZ). We found that while the devices based on SF-PDI_2 displayed a higher V_{oc} than those based on PCBM, they also suffered from lower J_{sc} and *FF*, leading to a lower overall PCE. The improved V_{oc} was due to the higher LUMO level of the SF-PDI_2, and higher E_{CT} of the SF-PDI_2 devices. This finding demonstrates one of the important advantages of NFAs over PCBM—the ability to easily tune the HOMO and LUMO levels of the material. However, the poor charge generation, transport, and collection of the SF-PDI_2 devices from the less pure domains, and low, imbalanced charge mobility led to a lower J_{sc} and *FF*. For the future design of new NFAs, improving the mobility and the way in which they pack with themselves and the donor polymer is important to achieving a higher J_{sc} and *FF*. Due to the anisotropic structure of NFAs, predicting their packing behavior and morphology is difficult; however, it is an important consideration when designing new materials. Ideally, an NFA will have an electron mobility of a similar magnitude or higher to that of fullerenes, while still maintaining the higher E_{CT}, and therefore V_{oc}, of their devices.

5.3 Impact of Donor Polymer Fluorination in NFA-based OPVs

In Chapter 3 we continued our investigation of NFA-based OPVs by studying the effect of donor polymer fluorination on device performance. Donor polymer fluorination is a commonly used method to improve efficiency in fullerene-based OPVs, however, in depth studies of the "F effect" in new NFA devices have not been completed. To investigate this "F effect," we chose a high performing NFA named ITIC as the electron acceptor, and paired it with

two donor polymers: non-fluorinated HTAZ and difluorinated FTAZ. In previous studies with these polymers in PCBM-based devices, it was found that fluorination led to an increase in PCE due mainly to an improvement in *FF* from increased hole mobility.[25,29] When these polymers were paired with ITIC as the electron acceptor, we observed a similar increase in *FF*. However, we also saw a large increase in the J_{sc}, to a much larger extent than in the PCBM devices. Upon further investigation, we determined that fluorination led to improved charge transport and extraction in the device as evidenced by the higher electron mobility, photocurrent, and charge collection probability. These results indicate that donor polymer fluorination is still a viable method to improve performance in NFA-based devices, and can lead to an even larger improvement than those seen in PCBM devices. When designing and testing new NFAs, it may be beneficial to pair them with a fluorinated donor polymer to obtain the highest possible efficiency.

5.4 Effect of Fluorination of Both the Donor and Acceptor Material

We continued our study of the "F effect" in non-fullerene acceptor OPVs in Chapter 4, focusing on the fluorination of the acceptor material. Recently, there have been reports of fluorinated NFAs, however, the effect of this fluorination is not well understood. Fluorinated NFAs can also be paired with fluorinated donor polymers such as FTAZ, and it is not yet understood how the degree of fluorination within the active layer blend will impact the performance. To gain insight into these questions, we chose two donor polymers (4'-FT-HTAZ and 4'-FT-FTAZ) and two NFAs (ITIC-Th and ITIC-Th1) with varying amounts of fluorination and paired them to obtain BHJ devices with a degree of fluorination ranging from 2F (4'-FT-HTAZ:ITIC-Th) to 6F (4'-FT-FTAZ:ITIC-Th1). We found that fluorination of the acceptor led

to a higher J_{sc} and *FF* due to an extended absorption range, higher and more balanced charge mobility, and a more favorable morphology. However, the V_{oc} of these devices was lower due to the lower LUMO level of the fluorinated acceptor (ITIC-Th1). Adding additional fluorine to the donor polymer deepens its HOMO level, increasing the V_{oc}. From these results it is clear that fluorination of the NFA can lead to an overall increase in the device efficiency, and should be considered in the design of future NFAs. However, to counteract the V_{oc} loss observed with fluorination, it may be important to pair the acceptor with a fluorinated donor to achieve a high J_{sc} and V_{oc} simultaneously.

5.5 Outlook

In this dissertation, we have shown that non-fullerene acceptors are promising alternatives to fullerene derivatives as the electron acceptor in organic photovoltaics. The development of new NFAs has led to a rapid increase in the power conversion efficiency of OPVs, approaching the efficiency of commercially available silicon devices. However, despite these advancements, there are still areas for improvement before OPV technologies can be commercialized. For example, many OPVs suffer from morphological instability, as the morphology of the bulk heterojunction is generally not the most thermodynamically stable state. Further understanding the ways in which NFAs interact with both themselves and the polymeric donor materials is important for the design of new BHJ systems to prevent long-term changes to the morphology that can decrease performance. Additionally, although OPVs can be processed on a large scale via roll-to-roll printing, many systems require toxic, halogenated solvents to obtain the optimal morphology and efficiency. Many researchers have begun developing new materials that can be processed in green, environmentally-friendly solvents such as alcohols and

water. Non-fullerene acceptors are at the forefront of research in both of these areas, as their structural versatility allows for the investigation of a large number of materials with a wide variety of properties. Gaining a better understanding of the structure-property relationships of both NFAs and donor polymers is critical to further increase the efficiency, improve the stability, and develop greener processing methods for OPVs, allowing for the widespread commercialization of these technologies.

APPENDIX A: SUPPORTING INFORMATION FOR CHAPTER 2

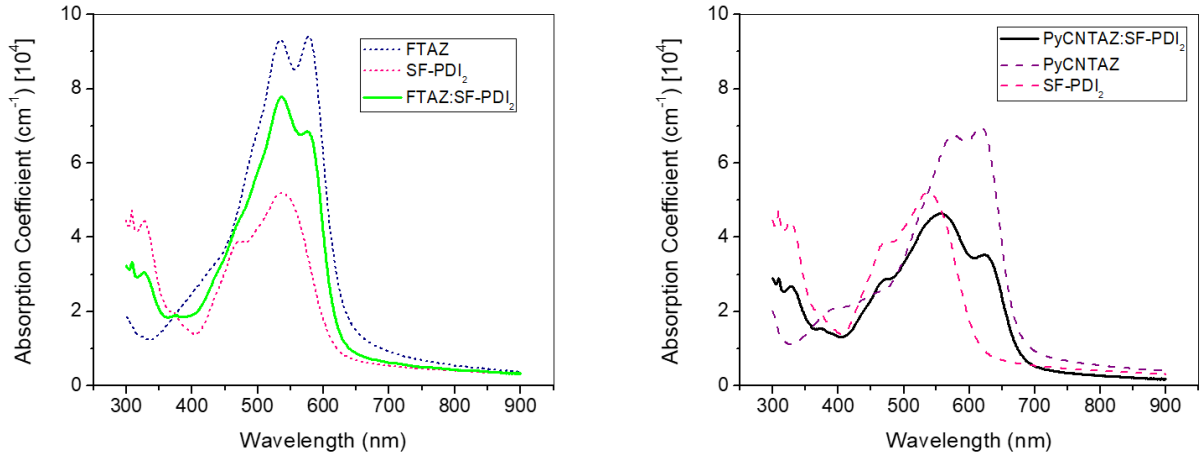

Figure A1 Absorption coefficients of neat materials and SF-PDI$_2$ blend films

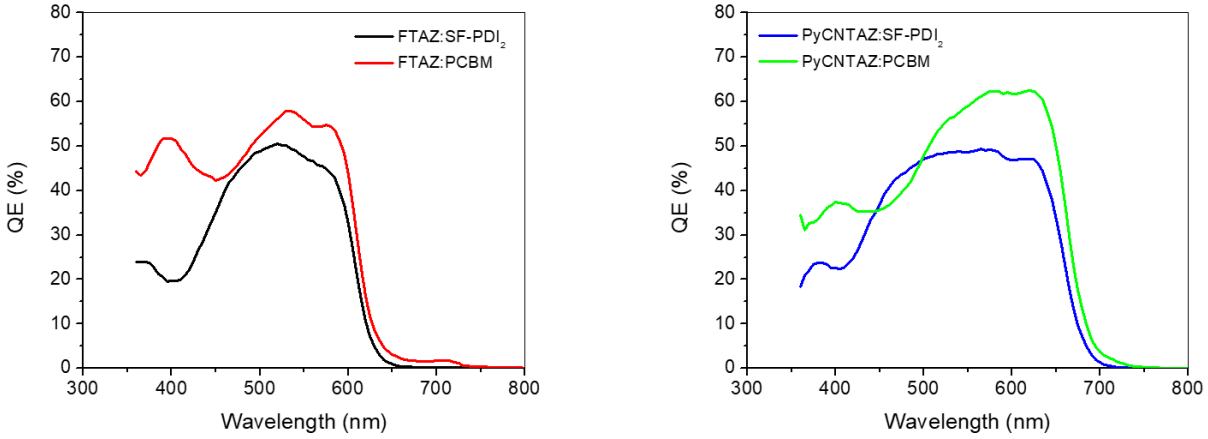

Figure A2 External quantum efficiencies of FTAZ (left) and PyCNTAZ (right) devices

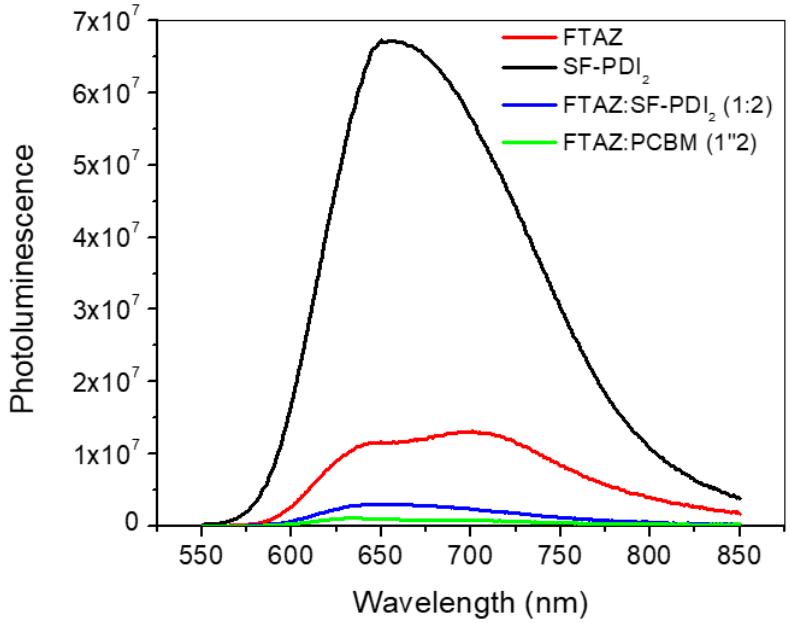

Figure A3 Photoluminescence of neat FTAZ and SF-PDI_2 films and FTAZ blends with D:A=1:2

APPENDIX B: SUPPORTING INFORATION FOR CHAPTER 3

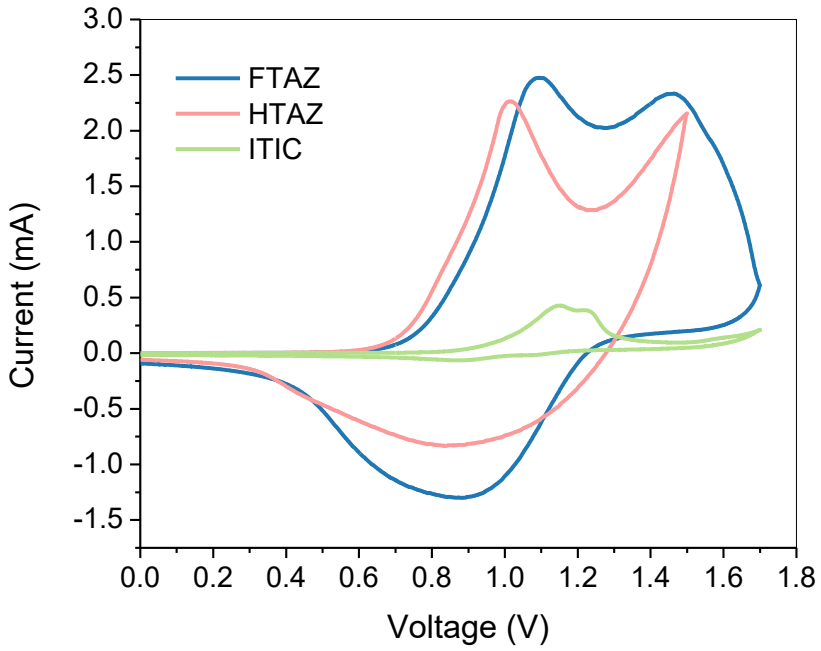

Figure B1 Cyclic voltammograms for FTAZ, HTAZ, and ITIC

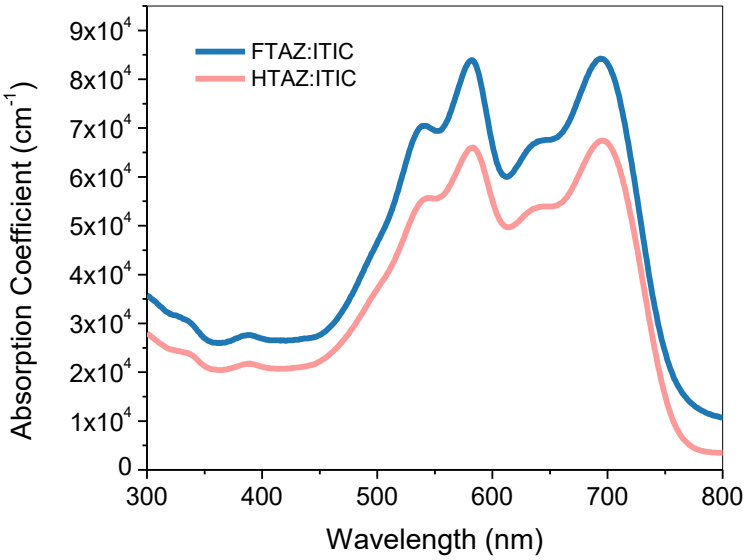

Figure B2 Absorption coefficient of FTAZ:ITIC and HTAZ:ITIC thin films

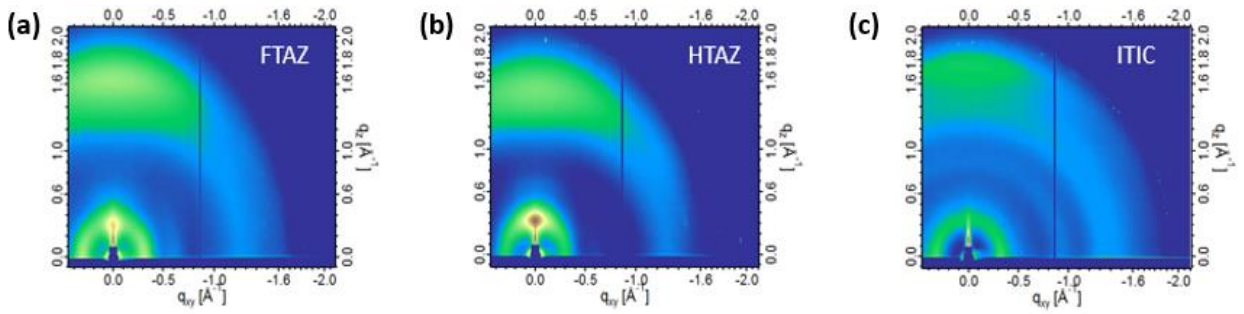

Figure B3 2D GIWAXS pattern of neat FTAZ, HTAZ, and ITIC films

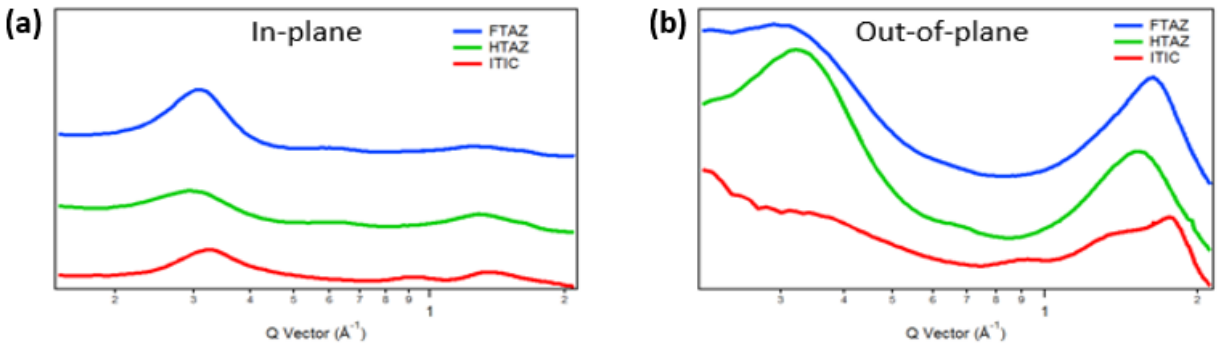

Figure B4 1D line scans for neat FTAZ, HTAZ, and ITIC films

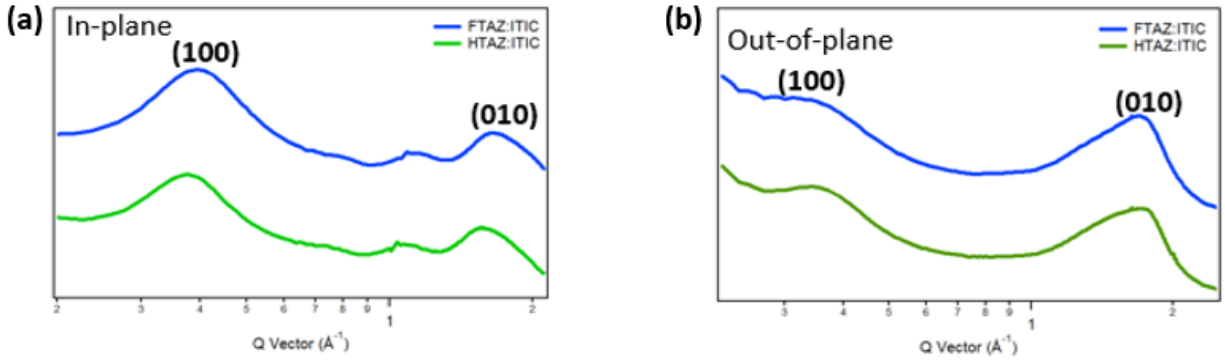

Figure B5 1D line scans for FTAZ:ITIC and HTAZ:ITIC blend films

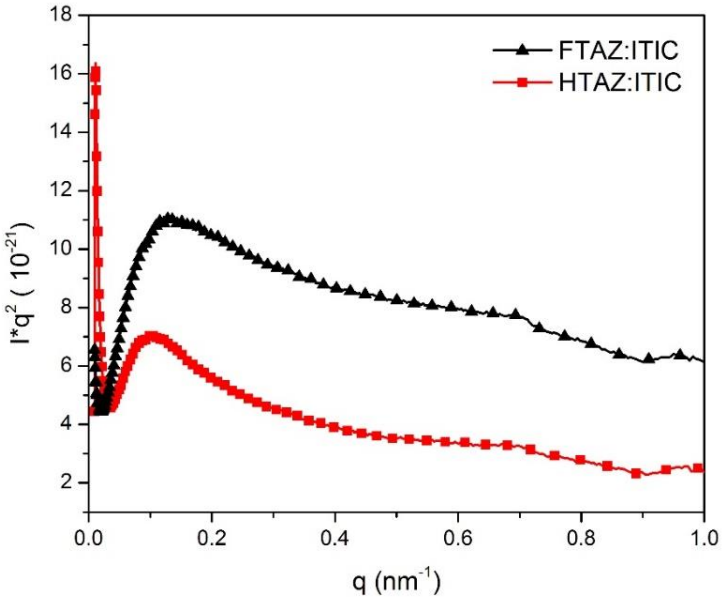

Figure B6 Lorentz-corrected RSoXS profiles of FTAZ:ITIC and HTAZ:ITIC blend films

APPENDIX C: SUPPORTING INFORMATION FOR CHAPTER 4

C.1 Materials Synthesis and Purification

All chemicals were purchased from commercial sources (Sigma-Aldrich, Fisher, Matrix, etc.) and were used as received except when specified. THF was distilled over sodium and benzophenone before use. Anhydrous o-xylene was purchased in sealed bottle from Sigma-Aldrich. Tris(dibenzylideneacetone)dipalladium(0)-chloroform adduct ($Pd_2dba_3 \cdot CHCl_3$) was purchased from Sigma-Aldrich and was recrystallized in chloroform/acetone. Tri(o-tolyl)phosphine ($P(o\text{-}tol)_3$) was recrystallized in hexanes. For reactions under argon, the glassware was evacuated and refilled with argon three times and charged with reactants. Microwave assisted polymerizations were conducted in a CEM Discover Benchmate microwave reactor.

C.2 Cyclic voltammetry

CV measurements were carried out on thin films using a Bioanalytical Systems (BAS) Epsilon potentiostat with a standard three-electrode configuration. A three electrode cell of a glassy carbon working electrode, Ag/Ag^+ reference electrode, and Pt counter electrode were used. Films of the donor polymers and NFAs were drop-cast onto the glassy carbon electrode from hot chloroform solution (2 mg/mL, with tetrabutylammonium hexafluorophosphate added at 100 wt%) and dried using a heat gun. 0.1 M solution of tetrabutylammonium hexafluorophosphate in anhydrous acetonitrile was used as a supporting electrolyte. Scans were carried out under argon atmosphere at a scan rate of 100 mV/s. The reference electrode was calibrated using a ferrocene/ferrocenium redox couple.

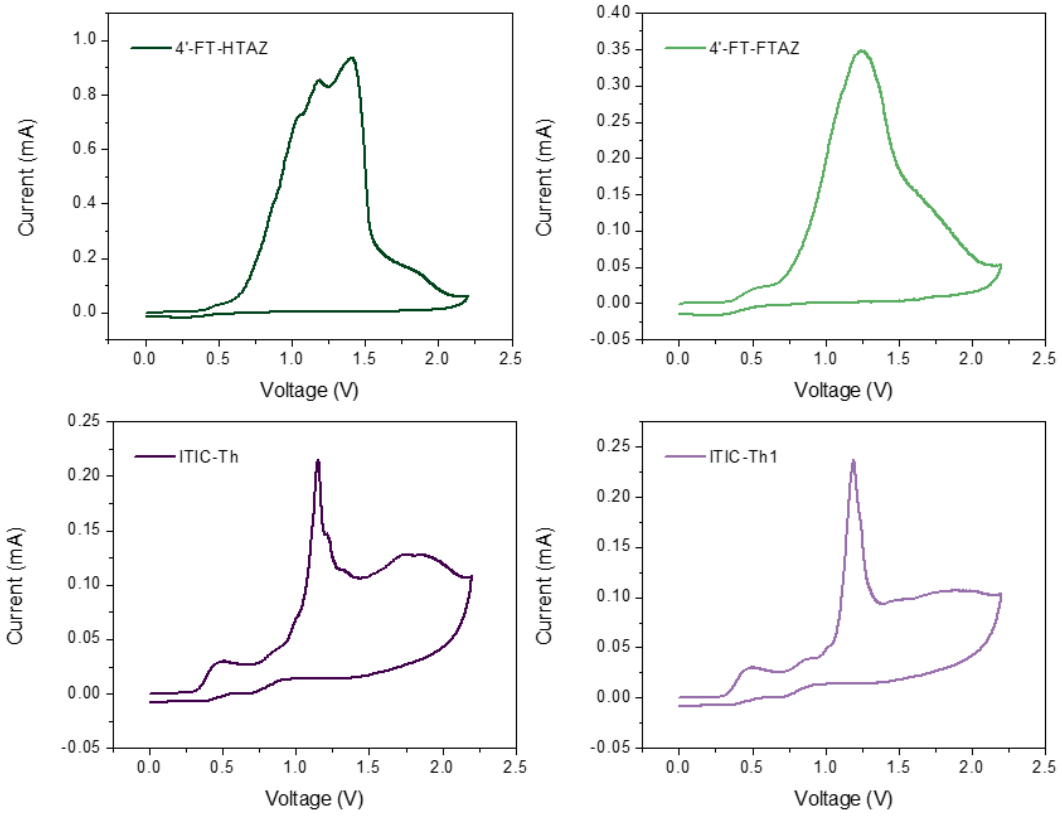

Figure C1 Cyclic voltammograms for 4'-FT-HTAZ, 4'-FT-FTAZ, ITIC-Th, and ITIC-Th1

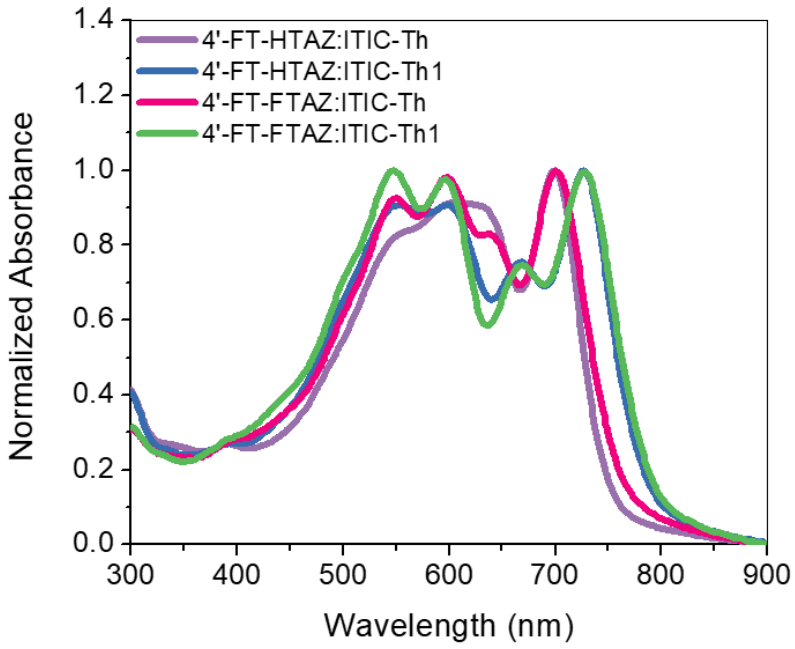

Figure C2 Normalized absorption for all four blend films

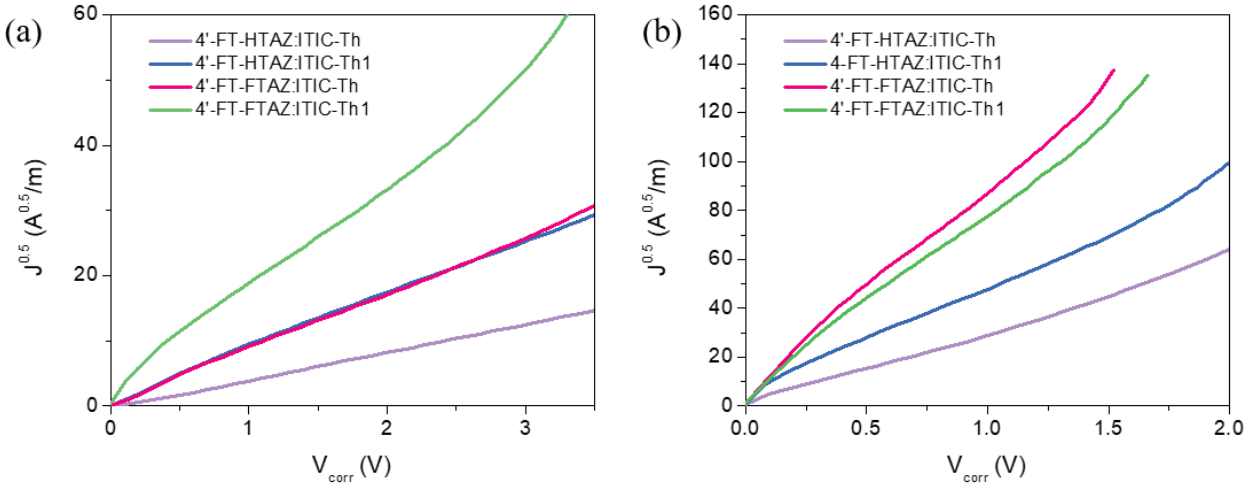

Figure C3 SCLC curves for a) electron and b) hole mobility for all four blend films

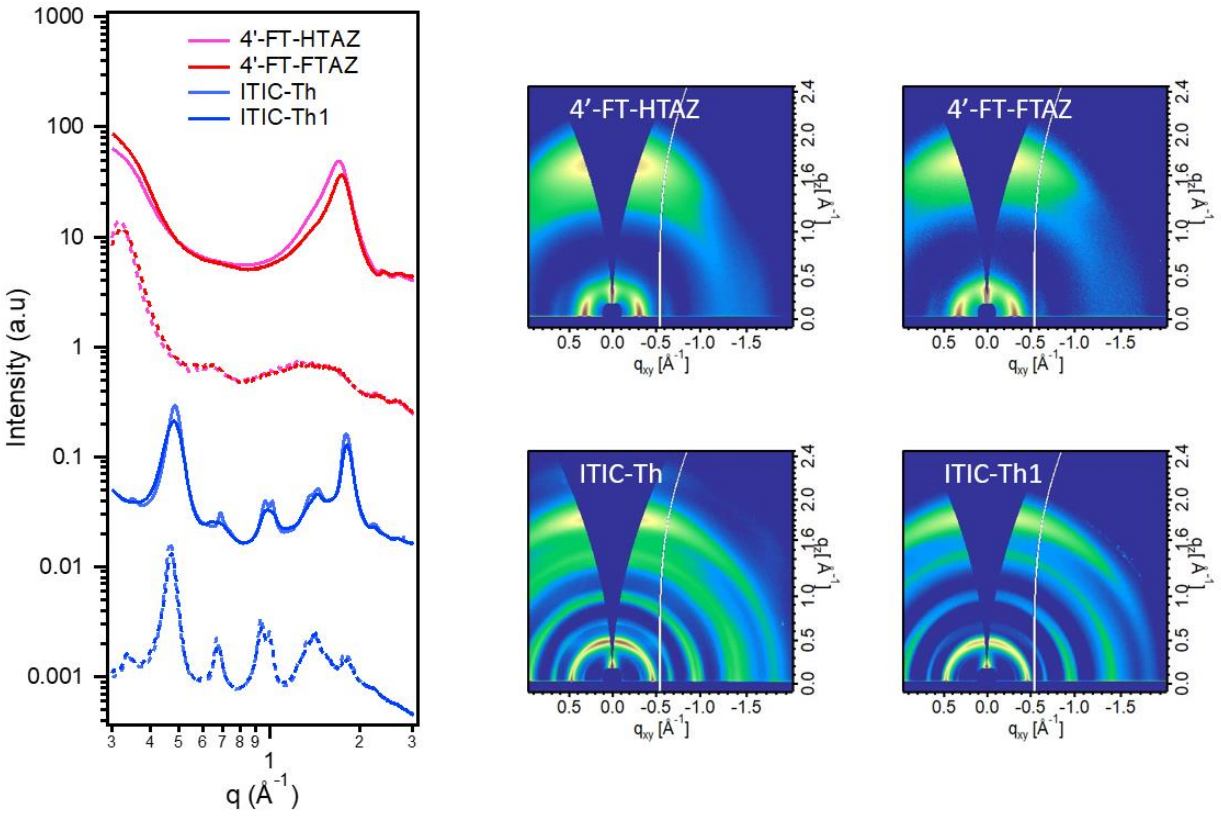

Figure C4 Sector averaged (+/-10˚) profiles (solid line: out-of-plane direction; dotted line: in-plane direction) and 2D GIWAXS plots for neat 4'-FT-HTAZ, 4'-FT-FTAZ, ITIC-Th, and ITIC-Th1 films

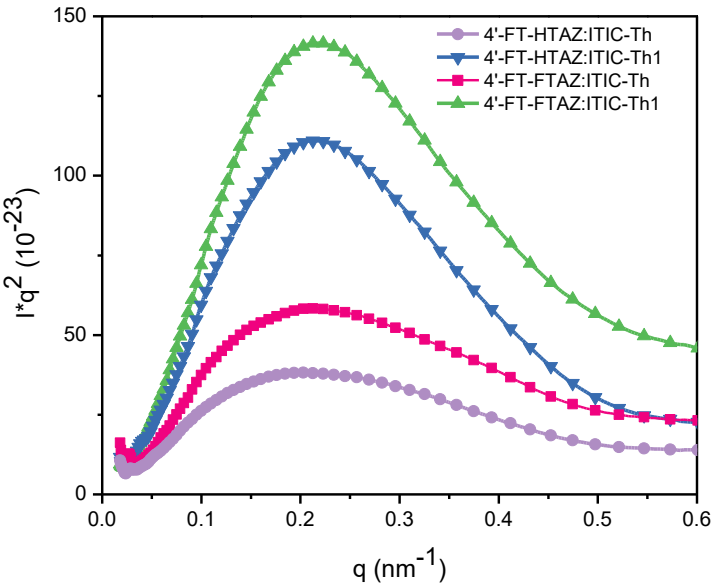

Figure C5 Thickness normalized and Lorentz-corrected RSoXS profiles of all four blend films

REFERENCES

(1) Tang, C. W. Two-layer Organic Photovoltaic Cell. *Appl. Phys. Lett.* **1986**, *48* (2), 183–185.

(2) Sariciftci, N. S.; Smilowitz, L.; Heeger, A. J.; Wudl, F. Photoinduced Electron Transfer from a Conducting Polymer to Buckminsterfullerene. *Science* **1992**, *258* (5087), 1474–1476.

(3) Yu, G.; Gao, J.; Hummelen, J. C.; Wudl, F.; Heeger, A. J. Polymer Photovoltaic Cells: Enhanced Efficiencies via a Network of Internal Donor-Acceptor Heterojunctions. *Science* **1995**, *270* (5243), 1789–1791.

(4) Dou, L.; You, J.; Hong, Z.; Xu, Z.; Li, G.; Street, R. A.; Yang, Y. 25th Anniversary Article: A Decade of Organic/Polymeric Photovoltaic Research. *Adv. Mater.* **2013**, *25* (46), 6642–6671.

(5) Zhou, H.; Yang, L.; You, W. Rational Design of High Performance Conjugated Polymers for Organic Solar Cells. *Macromolecules* **2012**, *45* (2), 607–632.

(6) Zhang, Q.; Kelly, M. A.; Bauer, N.; You, W. The Curious Case of Fluorination of Conjugated Polymers for Solar Cells. *Acc. Chem. Res.* **2017**, *50* (9), 2401–2409.

(7) Nielsen, C. B.; Holliday, S.; Chen, H.; Cryer, S. J.; Mcculloch, I. Non-Fullerene Electron Acceptors for Use in Organic Solar Cells. *Acc. Chem. Res.* **2015**, *48* (11), 2803–2812.

(8) Lin, Y.; Zhan, X. Designing Efficient Non-Fullerene Acceptors by Tailoring Extended Fused-Rings with Electron-Deficient Groups. *Adv. Energy Mater.* **2015**, *5*, 1501063.

(9) Yan, C.; Barlow, S.; Wang, Z.; Yan, H.; Jen, A. K.-Y.; Marder, S. R.; Zhan, X. Non-Fullerene Acceptors for Organic Solar Cells. *Nat. Rev. Mater.* **2018**, *3* (3), 18003.

(10) Lin, Y.; Wang, J.; Zhang, Z.; Bai, H.; Li, Y.; Zhu, D.; Zhan, X. An Electron Acceptor Challenging Fullerenes for Efficient Polymer Solar Cells. *Adv. Mater.* **2015**, *27* (7), 1170–1174.

(11) Yuan, J.; Zhang, Y.; Zhou, L.; Zhang, G.; Yip, H.-L.; Lau, T.; Lu, X.; Zhu, C.; Peng, H.; Johnson, P. A.; Leclerc, M.; Cao, Y.; Ulanski, J.; Li, Y.; Zou, Y. Single-Junction Organic Solar Cell with over 15% Efficiency Using Fused-Ring Acceptor with Electron-Deficient Core. *Joule* **2019**, *3*, 1–12.

(12) He, Y.; Li, Y. Fullerene Derivative Acceptors for High Performance Polymer Solar Cells. *Phys. Chem. Chem. Phys.* **2011**, *13* (6), 1970–1983.

(13) Li, S.; Zhang, Z.; Shi, M.; Li, C.-Z.; Chen, H. Molecular Electron Acceptors for Efficient Fullerene-Free Organic Solar Cells. *Phys. Chem. Chem. Phys.* **2017**, *19* (5), 3440–3458.

(14) Lin, Y.; Zhao, F.; He, Q.; Huo, L.; Wu, Y.; Parker, T. C.; Ma, W.; Sun, Y.; Wang, C.; Zhu, D.; Heeger, A. J.; Marder, S. R.; Zhan, X. A High-Performance Electron Acceptor with Thienyl Side Chains for Organic Photovoltaics. *J. Am. Chem. Soc.* **2016**, *138* (14), 4955–4961.

(15) Liu, T.; Meng, D.; Cai, Y.; Sun, X.; Li, Y.; Huo, L.; Liu, F.; Wang, Z.; Russell, T. P.; Sun, Y. High-Performance Non-Fullerene Organic Solar Cells Based on a Selenium-Containing Polymer Donor and a Twisted Perylene Bisimide Acceptor. *Adv. Sci.* **2016**, *3* (9), 1600117.

(16) Yao, H.; Chen, Y.; Qin, Y.; Yu, R.; Cui, Y.; Yang, B.; Li, S.; Zhang, K.; Hou, J. Design and Synthesis of a Low Bandgap Small Molecule Acceptor for Efficient Polymer Solar Cells. *Adv. Mater.* **2016**, *28* (37), 8283–8287.

(17) Gao, L.; Zhang, Z.; Bin, H.; Xue, L.; Yang, Y.; Wang, C.; Liu, F.; Russell, T. P.; Li, Y. High-Efficiency Nonfullerene Polymer Solar Cells with Medium Bandgap Polymer Donor and Narrow Bandgap Organic Semiconductor Acceptor. *Adv. Mater.* **2016**, *28*, 8288–8295.

(18) Zhao, W.; Qian, D.; Zhang, S.; Li, S.; Inganäs, O.; Gao, F.; Hou, J. Fullerene-Free Polymer Solar Cells with over 11% Efficiency and Excellent Thermal Stability. *Adv. Mater.* **2016**, *28* (23), 4734–4739.

(19) Li, S.; Ye, L.; Zhao, W.; Zhang, S.; Mukherjee, S.; Ade, H.; Hou, J. Energy-Level Modulation of Small-Molecule Electron Acceptors to Achieve over 12% Efficiency in Polymer Solar Cells. *Adv. Mater.* **2016**, *28*, 9423–9429.

(20) He, Z.; Xiao, B.; Liu, F.; Wu, H.; Yang, Y.; Xiao, S.; Wang, C.; Russell, T. P.; Cao, Y. Single-Junction Polymer Solar Cells with High Efficiency and Photovoltage. *Nat. Photonics* **2015**, *9* (3), 174–179.

(21) Vohra, V.; Kawashima, K.; Kakara, T.; Koganezawa, T.; Osaka, I.; Takimiya, K.; Murata, H. Efficient Inverted Polymer Solar Cells Employing Favourable Molecular Orientation. *Nat. Photonics* **2015**, *9*, 403–409.

(22) Zhao, J.; Li, Y.; Yang, G.; Jiang, K.; Lin, H.; Ade, H.; Ma, W.; Yan, H. Efficient Organic Solar Cells Processed from Hydrocarbon Solvents. *Nat. Energy* **2016**, *1* (2), 15027.

(23) Lin, Y.; Zhan, X. Non-Fullerene Acceptors for Organic Photovoltaics: An Emerging Horizon. *Mater. Horizons* **2014**, *1* (5), 470–488.

(24) Lakhwani, G.; Rao, A.; Friend, R. H. Bimolecular Recombination in Organic Photovoltaics. *Annu. Rev. Phys. Chem.* **2014**, *65* (1), 557–581.

(25) Li, W.; Albrecht, S.; Yang, L.; Roland, S.; Tumbleston, J. R.; McAfee, T.; Yan, L.; Kelly, M. A.; Ade, H.; Neher, D.; You, W. Mobility-Controlled Performance of Thick Solar Cells Based on Fluorinated Copolymers. *J. Am. Chem. Soc.* **2014**, *136* (44), 15566–15576.

(26) Lin, Y.; Cheng, P.; Li, Y.; Zhan, X. A 3D Star-Shaped Non-Fullerene Acceptor for Solution-Processed Organic Solar Cells with a High Open-Circuit Voltage of 1.18 V. *Chem. Commun.* **2012**, *48* (39), 4773.

(27) Meng, D.; Sun, D.; Zhong, C.; Liu, T.; Fan, B.; Huo, L.; Li, Y.; Jiang, W.; Choi, H.; Kim, T.; Kim, J. Y.; Sun, Y.; Wang, Z.; Heeger, A. J. High-Performance Solution-Processed Non-Fullerene Organic Solar Cells Based on Selenophene-Containing Perylene Bisimide Acceptor. *J. Am. Chem. Soc.* **2016**, *138* (1), 375–380.

(28) Zhao, J.; Li, Y.; Lin, H.; Liu, Y.; Jiang, K.; Mu, C.; Ma, T.; Lin Lai, J. Y.; Hu, H.; Yu, D.; Yan, H. High-Efficiency Non-Fullerene Organic Solar Cells Enabled by a Difluorobenzothiadiazole-Based Donor Polymer Combined with a Properly Matched Small Molecule Acceptor. *Energy Environ. Sci.* **2015**, *8* (2), 520–525.

(29) Price, S. C.; Stuart, A. C.; Yang, L. G.; Zhou, H. X.; You, W. Fluorine Substituted Conjugated Polymer of Medium Bandwidth Yield 7% Efficiency in Polymer-Fullerene Solar Cells. *J. Am. Chem. Soc.* **2011**, *133*, 4625–4631.

(30) Li, W.; Yan, L.; Zhou, H.; You, W. A General Approach toward Electron Deficient Triazole Units to Construct Conjugated Polymers for Solar Cells. *Chem. Mater.* **2015**, *27* (18), 6470–6476.

(31) Li, W.; Yang, L.; Tumbleston, J. R.; Yan, L.; Ade, H.; You, W. Controlling Molecular Weight of a High Efficiency Donor-Acceptor Conjugated Polymer and Understanding Its Significant Impact on Photovoltaic Properties. *Adv. Mater.* **2014**, *26* (26), 4456–4462.

(32) Hoke, E. T.; Vandewal, K.; Bartelt, J. A.; Mateker, W. R.; Douglas, J. D.; Noriega, R.; Graham, K. R.; Fréchet, J. M. J.; Salleo, A.; Mcgehee, M. D. Recombination in Polymer:Fullerene Solar Cells with Open-Circuit Voltages Approaching and Exceeding 1.0 V. *Adv. Energy Mater.* **2013**, *3* (2), 220–230.

(33) Vandewal, K.; Tvingstedt, K.; Gadisa, A.; Inganäs, O.; Manca, J. V. On the Origin of the Open-Circuit Voltage of Polymer--Fullerene Solar Cells. *Nat. Mater.* **2009**, *8*, 904–909.

(34) Vandewal, K.; Tvingstedt, K.; Gadisa, A.; Inganäs, O.; Manca, J. V. Relating the Open-Circuit Voltage to Interface Molecular Properties of Donor:Acceptor Bulk Heterojunction Solar Cells. *Phys. Rev. B* **2010**, *81* (12), 125204.

(35) Faist, M. A.; Kirchartz, T.; Gong, W.; Ashraf, R. S.; Mcculloch, I.; De Mello, J. C.; Ekins-Daukes, N. J.; Bradley, D. D. C.; Nelson, J. Competition between the Charge Transfer State and the Singlet States of Donor or Acceptor Limiting the Efficiency in Polymer:Fullerene Solar Cells. *J. Am. Chem. Soc.* **2011**, *134* (1), 685–692.

(36) Liu, J.; Chen, S.; Qian, D.; Gautam, B.; Yang, G.; Zhao, J.; Bergqvist, J.; Zhang, F.; Ma, W.; Ade, H.; Inganäs, O.; Gundogdu, K.; Gao, F.; Yan, H. Fast Charge Separation in a Non-Fullerene Organic Solar Cell with a Small Driving Force. *Nat. Energy* **2016**, *1* (9), 16089.

(37) Kyaw, A. K. K.; Wang, D. H.; Gupta, V.; Leong, W. L.; Ke, L.; Bazan, G. C.; Heeger, A. J. Intensity Dependence of Current À Voltage Characteristics and Recombination in High-E Ffi Ciency. *ACS Nano* **2013**, No. 5, 4569–4577.

(38) Lu, L.; Zheng, T.; Xu, T.; Zhao, D.; Yu, L. Mechanistic Studies of Effect of Dispersity on the Photovoltaic Performance of PTB7 Polymer Solar Cells. *Chem. Mater.* **2015**, *27* (2), 537–543.

(39) Cowan, S. R.; Roy, A.; Heeger, A. J. Recombination in Polymer-Fullerene Bulk Heterojunction Solar Cells. *Phys. Rev. B* **2010**, *82* (24), 245207.

(40) Brus, V. V. Light Dependent Open-Circuit Voltage of Organic Bulk Heterojunction Solar Cells in the Presence of Surface Recombination. *Org. Electron.* **2016**, *29*, 1–6.

(41) Solak, S.; Blom, P. W. M.; Wetzelaer, G. A. H. Effect of Non-Ohmic Contacts on the Light-Intensity Dependence of the Open-Circuit Voltage in Organic Solar Cells. *Appl. Phys. Lett.* **2016**, *109* (5), 053302.

(42) Blom, P. W. M.; Mihailetchi, V. D.; Koster, L. J. A.; Markov, D. E. Device Physics of Polymer:Fullerene Bulk Heterojunction Solar Cells. *Adv. Mater.* **2007**, *19* (12), 1551–1566.

(43) Yang, L.; Tumbleston, J.; Zhou, H.; Ade, H.; You, W. Disentangling the Impact of Side Chains and Fluorine Substituents of Conjugated Donor Polymers on the Performance of Photovoltaic Blends. *Energy Environ. Sci.* **2012**, 316–326.

(44) Proctor, C. M.; Love, J. A.; Nguyen, T.-Q. Mobility Guidelines for High Fill Factor Solution-Processed Small Molecule Solar Cells. *Adv. Mater.* **2014**, *26* (34), 5957–5961.

(45) Beaujuge, P. M.; Fréchet, J. M. J. Molecular Design and Ordering Effects in π-Functional Materials for Transistor and Solar Cell Applications. *J. Am. Chem. Soc.* **2011**, *133* (50), 20009–20029.

(46) Bartelt, J. A.; Beiley, Z. M.; Hoke, E. T.; Mateker, W. R.; Douglas, J. D.; Collins, B. A.; Tumbleston, J. R.; Graham, K. R.; Amassian, A.; Ade, H.; Fréchet, J. M. J.; Toney, M. F.; McGehee, M. D. The Importance of Fullerene Percolation in the Mixed Regions of Polymer-Fullerene Bulk Heterojunction Solar Cells. *Adv. Energy Mater.* **2013**, *3* (3), 364–374.

(47) Carpenter, J. H.; Hunt, A.; Ade, H. Characterizing Morphology in Organic Systems with Resonant Soft X-Ray Scattering. *J. Electron Spectros. Relat. Phenomena* **2015**, *200*, 2–14.

(48) Mukherjee, S.; Jiao, X.; Ade, H. Charge Creation and Recombination in Multi-Length Scale Polymer:Fullerene BHJ Solar Cell Morphologies. *Adv. Energy Mater.* **2016**, *6* (18), 1600699.

(49) Ye, L.; Zhao, W.; Li, S.; Mukherjee, S.; Carpenter, J. H.; Awartani, O.; Jiao, X.; Hou, J.; Ade, H. High-Efficiency Nonfullerene Organic Solar Cells: Critical Factors That Affect

Complex Multi-Length Scale Morphology and Device Performance. *Adv. Energy Mater.* **2017**, *7*, 1602000.

(50) Li, S.; Ye, L.; Zhao, W.; Zhang, S.; Mukherjee, S.; Ade, H.; Hou, J. Energy-Level Modulation of Small-Molecule Electron Acceptors to Achieve over 12% Efficiency in Polymer Solar Cells. *Adv. Mater.* **2016**, *28*, 9423–9429.

(51) Zhou, Y.; Fuentes-Hernandez, C.; Shim, J.; Meyer, J.; Giordano, A. J.; Li, H.; Winget, P.; Papadopoulos, T.; Cheun, H.; Kim, J.; Fenoll, M.; Dindar, A.; Haske, W.; Najafabadi, E.; Khan, T. M.; Sojoudi, H.; Barlow, S.; Graham, S.; Bredas, J.-L.; Marder, S. R.; Kahn, A.; Kippelen, B. A Universal Method to Produce Low-Work Function Electrodes for Organic Electronics. *Science (80-.).* **2012**, *336* (6079), 327–332.

(52) Hexemer, A.; Bras, W.; Gossinger, J.; Schaible, E.; Gann, E.; Kirian, R.; MacDowell, A.; Church, M.; Rude, B.; Padmore, H. A SAXS/WAXS/GISAXS Beamline with Multilayer Monochromator. *J. Phys. Conf. Ser.* **2010**, *247* (1), 012007.

(53) Gann, E.; Young, A. T.; Collins, B. A.; Yan, H.; Nasiatka, J.; Padmore, H. A.; Ade, H.; Hexemer, A.; Wang, C. Soft X-Ray Scattering Facility at the Advanced Light Source with Real-Time Data Processing and Analysis. *Rev. Sci. Instrum.* **2012**, *83* (4), 045110.

(54) Kilcoyne, A. L. D.; Tyliszczak, T.; Steele, W. F.; Fakra, S.; Hitchcock, P.; Franck, K.; Anderson, E.; Harteneck, B.; Rightor, E. G.; Mitchell, G. E.; Hitchcock, A. P.; Yang, L.; Warwick, T.; Ade, H. Interferometer-Controlled Scanning Transmission X-Ray Microscopes at the Advanced Light Source. *J. Synchrotron Rad* **2003**, *10*, 125–136.

(55) Ilavsky, J. Nika : Software for Two-Dimensional Data Reduction. *J. Appl. Crystallogr.* **2012**, *45* (2), 324–328.

(56) Leclerc, N.; Chávez, P.; Ibraikulov, O.; Heiser, T.; Lévêque, P. Impact of Backbone Fluorination on π-Conjugated Polymers in Organic Photovoltaic Devices: A Review. *Polymers (Basel).* **2016**, *8* (1), 11.

(57) Xu, X.-P.; Li, Y.; Luo, M.-M.; Peng, Q. Recent Progress towards Fluorinated Copolymers for Efficient Photovoltaic Applications. *Chinese Chem. Lett.* **2016**, *27*, 1241–1249.

(58) Meyer, F. Fluorinated Conjugated Polymers in Organic Bulk Heterojunction Photovoltaic Solar Cells. *Prog. Polym. Sci.* **2015**, *47*, 70–91.

(59) Lin, Y.; Zhan, X. Oligomer Molecules for Efficient Organic Photovoltaics. *Acc. Chem. Res.* **2016**, *49* (2), 175–183.

(60) Dai, S.; Zhao, F.; Zhang, Q.; Lau, T.-K.; Li, T.; Liu, K.; Ling, Q.; Wang, C.; Lu, X.; You, W.; Zhan, X. Fused Nonacyclic Electron Acceptors for Efficient Polymer Solar Cells. *J. Am. Chem. Soc.* **2017**, *139* (3), 1336–1343.

(61) Zhao, F.; Dai, S.; Wu, Y.; Zhang, Q.; Wang, J.; Jiang, L.; Ling, Q.; Wei, Z.; Ma, W.; You, W.; Wang, C.; Zhan, X. Single-Junction Binary-Blend Nonfullerene Polymer Solar Cells

with 12.1% Efficiency. *Adv. Mater.* **2017**, *29* (18), 1700144.

(62) Wang, J.; Wang, W.; Wang, X.; Wu, Y.; Zhang, Q.; Yan, C.; Ma, W.; You, W.; Zhan, X. Enhancing Performance of Nonfullerene Acceptors via Side-Chain Conjugation Strategy. *Adv. Mater.* **2017**, 1702125.

(63) Yao, H.; Ye, L.; Hou, J.; Jang, B.; Han, G.; Cui, Y.; Su, G. M.; Wang, C.; Gao, B.; Yu, R.; Zhang, H.; Yi, Y.; Woo, H. Y.; Ade, H.; Hou, J. Achieving Highly Efficient Nonfullerene Organic Solar Cells with Improved Intermolecular Interaction and Open-Circuit Voltage. *Adv. Mater.* **2017**, *29* (21), 1700254.

(64) Yi, Y.-Q.-Q.; Feng, H.; Chang, M.; Zhang, H.; Wan, X.; Li, C.; Chen, Y.; Zhang, H.; Li, C.; Hou, J.; Chen, Y.; Marder, S. R.; Zhan, X.; Amassian, A.; Salleo, A.; Kirchartz, T.; Durrant, J. R.; McCulloch, I. New Small-Molecule Acceptors Based on Hexacyclic Naphthalene(Cyclopentadithiophene) for Efficient Non-Fullerene Organic Solar Cells. *J. Mater. Chem. A* **2017**, *5* (33), 17204–17210.

(65) Guo, B.; Li, W.; Guo, X.; Meng, X.; Ma, W.; Zhang, M.; Li, Y. High Efficiency Nonfullerene Polymer Solar Cells with Thick Active Layer and Large Area. *Adv. Mater.* **2017**, 1702291.

(66) Lin, F.; Huang, W.; Sun, H.; Xin, J.; Zeng, H.; Yang, T.; Li, M.; Zhang, X.; Ma, W.; Liang, Y. Thieno[3,4- *c*]Pyrrole-4,6(5 *H*)-Dione Polymers with Optimized Energy Level Alignments for Fused-Ring Electron Acceptor Based Polymer Solar Cells. *Chem. Mater.* **2017**, *29* (13), 5636–5645.

(67) Wang, W.; Yan, C.; Lau, T.-K.; Wang, J.; Liu, K.; Fan, Y.; Lu, X.; Zhan, X. Fused Hexacyclic Nonfullerene Acceptor with Strong Near-Infrared Absorption for Semitransparent Organic Solar Cells with 9.77% Efficiency. *Adv. Mater.* **2017**, *29* (31), 1701308.

(68) Bao, X.; Zhang, Y.; Wang, J.; Zhu, D.; Yang, C.; Li, Y.; Yang, C.; Xu, J.; Yang, R. High Extinction Coefficient Thieno[3,4- *b*]Thiophene-Based Copolymer for Efficient Fullerene-Free Solar Cells with Large Current Density. *Chem. Mater.* **2017**, *29* (16), 6766–6771.

(69) Yu, T.; Xu, X.; Zhang, G.; Wan, J.; Li, Y.; Peng, Q. Wide Bandgap Copolymers Based on Quinoxalino[6,5-f].Quinoxaline for Highly Efficient Nonfullerene Polymer Solar Cells. *Adv. Funct. Mater.* **2017**, *27* (28), 1701491.

(70) Zhao, W.; Li, S.; Yao, H.; Zhang, S.; Zhang, Y.; Yang, B.; Hou, J. Molecular Optimization Enables over 13% Efficiency in Organic Solar Cells. *J. Am. Chem. Soc.* **2017**, *139* (21), 7148–7151.

(71) Li, Z.; Jiang, K.; Yang, G.; Lai, J. Y. L.; Ma, T.; Zhao, J.; Ma, W.; Yan, H. Donor Polymer Design Enables Efficient Non-Fullerene Organic Solar Cells. *Nat. Commun.* **2016**, *7*, 13094.

(72) Bauer, N.; Zhang, Q.; Zhao, J.; Ye, L.; Kim, J.-H.; Constantinou, I.; Yan, L.; So, F.; Ade, H.; Yan, H.; You, W. Comparing Non-Fullerene Acceptors with Fullerene in Polymer Solar Cells: A Case Study with FTAZ and PyCNTAZ. *J. Mater. Chem. A* **2017**, *5* (10), 4886–4893.

(73) Ye, L.; Xiong, Y.; Li, S.; Ghasemi, M.; Balar, N.; Turner, J.; Gadisa, A.; Hou, J.; O'Connor, B. T.; Ade, H. Precise Manipulation of Multilength Scale Morphology and Its Influence on Eco-Friendly Printed All-Polymer Solar Cells. *Adv. Funct. Mater.* **2017**, *10*, 1702016.

(74) Mukherjee, S.; Herzing, A.; Zhao, D.; Wu, Q.; Yu, L.; Ade, H.; DeLongchamp, D. M.; Richter, L. J. Morphological Characterization of Fullerene and Fullerene-Free Organic Photovoltaics by Combined Real and Reciprocal Space Techniques. *J. Mater. Res.* **2017**, *32* (10), 1921–1934.

(75) Zhang, Q.; Yan, L.; Jiao, X.; Peng, Z.; Liu, S.; Rech, J. J.; Klump, E.; Ade, H.; So, F.; You, W. Fluorinated Thiophene Units Improve Photovoltaic Device Performance of Donor–Acceptor Copolymers. *Chem. Mater.* **2017**, *29* (14), 5990–6002.

(76) Leclerc, N.; Chávez, P.; Ibraikulov, O.; Heiser, T.; Lévêque, P.; Leclerc, N.; Chávez, P.; Ibraikulov, O. A.; Heiser, T.; Lévêque, P. Impact of Backbone Fluorination on π-Conjugated Polymers in Organic Photovoltaic Devices: A Review. *Polymers (Basel).* **2016**, *8* (1), 11.

(77) Meyer, F. Fluorinated Conjugated Polymers in Organic Bulk Heterojunction Photovoltaic Solar Cells. *Prog. Polym. Sci.* **2015**, *47*, 70–91.

(78) Xu, X.-P.; Li, Y.; Luo, M.-M.; Peng, Q. Recent Progress towards Fluorinated Copolymers for Efficient Photovoltaic Applications. *Chinese Chem. Lett.* **2016**, *27* (8), 1241–1249.

(79) Liang, Y.; Feng, D.; Wu, Y.; Tsai, S.-T.; Li, G.; Ray, C.; Yu, L. Highly Efficient Solar Cell Polymers Developed via Fine-Tuning of Structural and Electronic Properties. *J. Am. Chem. Soc.* **2009**, *131* (22), 7792–7799.

(80) Chen, H.-Y.; Hou, J.; Zhang, S.; Liang, Y.; Yang, G.; Yang, Y.; Yu, L.; Wu, Y.; Li, G. Polymer Solar Cells with Enhanced Open-Circuit Voltage and Efficiency. *Nat. Photonics* **2009**, *3* (11), 649–653.

(81) Zhou, H.; Yang, L.; Stuart, A. C.; Price, S. C.; Liu, S.; You, W. Development of Fluorinated Benzothiadiazole as a Structural Unit for a Polymer Solar Cell of 7 % Efficiency. *Angew. Chemie Int. Ed.* **2011**, *50* (13), 2995–2998.

(82) Price, S. C.; Stuart, A. C.; Yang, L.; Zhou, H.; You, W. Fluorine Substituted Conjugated Polymer of Medium Band Gap Yields 7% Efficiency in Polymer−Fullerene Solar Cells. *J. Am. Chem. Soc.* **2011**, *133* (12), 4625–4631.

(83) Zhang, Q.; Yan, L.; Jiao, X.; Peng, Z.; Liu, S.; Rech, J. J.; Klump, E.; Ade, H.; So, F.; You, W. Fluorinated Thiophene Units Improve Photovoltaic Device Performance of

Donor–Acceptor Copolymers. *Chem. Mater.* **2017**, *29* (14), 5990–6002.

(84) Long, X.; Dou, C.; Liu, J.; Wang, L. Fine-Tuning LUMO Energy Levels of Conjugated Polymers Containing a B←N Unit. *Macromolecules* **2017**, *50* (21), 8521–8528.

(85) Cai, M.; Bao, X.; Liu, Y. F.; Li, C.; Wang, X.; Lan, Z.; Yang, R.; Wan, X. Unexpected Opposite Influences of Para vs Ortho Backbone Fluorination on the Photovoltaic Performance of a Wide-Bandgap Conjugated Polymer. *Chem. Mater.* **2017**, *29* (21), 9162–9170.

(86) Yu, J.; Yang, J.; Zhou, X.; Yu, S.; Tang, Y.; Wang, H.; Chen, J.; Zhang, S.; Guo, X. Phthalamide-Based Wide Bandgap Donor Polymers for Efficient Non-Fullerene Solar Cells. *Macromolecules* **2017**, *50* (22), 8928–8937.

(87) Deng, D.; Zhang, Y.; Zhang, J.; Wang, Z.; Zhu, L.; Fang, J.; Xia, B.; Wang, Z.; Lu, K.; Ma, W.; Wei, Z. Fluorination-Enabled Optimal Morphology Leads to over 11% Efficiency for Inverted Small-Molecule Organic Solar Cells. *Nat. Commun.* **2016**, *7*, 1–9.

(88) Zhang, G.; Xu, X.; Bi, Z.; Ma, W.; Tang, D.; Li, Y.; Peng, Q. Fluorinated and Alkylthiolated Polymeric Donors Enable Both Efficient Fullerene and Nonfullerene Polymer Solar Cells. *Adv. Funct. Mater.* **2018**, *28* (10), 1706404.

(89) Peng, R.; Guo, H.; Xiao, J.; Wang, G.; Tan, S.; Zhao, B.; Guo, X.; Li, Y. Synergistic Effect of Fluorine Substitution and Thio-Alkylation on Photovoltaic Performances of Alternating Conjugated Polymers Based on Alkylthio-Substituted Benzothiadiazole-Quaterthiophene. *ACS Appl. Energy Mater.* **2018**, *1*, 2192–2199.

(90) Weng, K.; Xue, X.; Qi, F.; Zhang, Y.; Huo, L.; Zhang, J.; Wei, D.; Wan, M.; Sun, Y. Synergistic E Ff Ects of Fluorination and Alkylthiolation on the Photovoltaic Performance of the Poly(Benzodithiophene- Benzothiadiazole) Copolymers. *ACS Appl. Energy Mater.* **2018**, *1* (9), 4686–4694.

(91) Gao, Y.; Wang, Z.; Zhang, J.; Zhang, H.; Lu, K.; Guo, F.; Wei, Z.; Yang, Y.; Zhao, L.; Zhang, Y. Wide-Bandgap Conjugated Polymers Based on Alkylthiofuran-Substituted Benzo[1,2 - B :4,5 - b ′]Difuran for E Ffi Cient Fullerene-Free Polymer Solar Cells. *Macromolecules* **2018**, *51* (7), 2498–2505.

(92) Song, S.; Kim, S.; Kim, W.; Park, S. S.; Park, S. H.; Jin, Y. Synthesis and Photovoltaic Properties of Copolymers with a Fluoro Quinoxaline Unit. *J. Polym. Sci. Part A Polym. Chem.* **2018**, *56* (8), 821–830.

(93) Bauer, N.; Zhang, Q.; Zhu, J.; Peng, Z.; Yan, L.; Zhu, C.; Ade, H.; Zhan, X.; You, W. Donor Polymer Fluorination Doubles the Efficiency in Non-Fullerene Organic Photovoltaics. *J. Mater. Chem. A* **2017**, *5* (43), 22536–22541.

(94) Yang, J.; Uddin, M. A.; Tang, Y.; Wang, Y.; Wang, Y.; Su, H.; Gao, R.; Chen, Z.; Dai, J.; Woo, H. Y.; Guo, X. Quinoxaline-Based Wide Band Gap Polymers for Efficient Nonfullerene Organic Solar Cells with Large Open-Circuit Voltages. *ACS Appl. Mater.*

Interfaces **2018**, *10*, 23235–23246.

(95) Xie, R.; Ying, L.; Liao, H.; Chen, Z.; Huang, F.; Cao, Y. Efficient Non-Fullerene Organic Solar Cells Enabled by Sequential Fluorination of Small-Molecule Electron Acceptors. *Front. Chem.* **2018**, *6*, 303.

(96) Fan, Q.; Su, W.; Wang, Y.; Guo, B.; Jiang, Y.; Guo, X.; Liu, F.; Russell, T. P.; Zhang, M.; Li, Y. Synergistic Effect of Fluorination on Both Donor and Acceptor Materials for High Performance Non-Fullerene Polymer Solar Cells with 13.5% Efficiency. *Sci. China Chem.* **2018**, *61* (5), 531–537.

(97) Lin, Z.; Huang, K.; Wang, Z.; Chen, X.; Sun, J.; Xu, Z.; He, T.; Yin, S.; Li, M.; Zhang, Q.; Qiu, H. Alkyl Side-Chain and Fluorination Engineering in the Indeno[1,2-b]Fluorene-Based Small-Molecule Acceptors for Efficient Non-Fullerene Organic Solar Cells. *Dye. Pigment.* **2019**, *160*, 432–438.

(98) Lee, J.; Ko, S.-J.; Seifrid, M.; Lee, H.; McDowell, C.; Luginbuhl, B. R.; Karki, A.; Cho, K.; Nguyen, T.-Q.; Bazan, G. C. Design of Nonfullerene Acceptors with Near-Infrared Light Absorption Capabilities. *Adv. Energy Mater.* **2018**, *8* (26), 1801209.

(99) Li, T.; Zhang, H.; Xiao, Z.; Rech, J. J.; Niu, H.; You, W.; Ding, L. A Carbon–oxygen-Bridged Hexacyclic Ladder-Type Building Block for Low-Bandgap Nonfullerene Acceptors. *Mater. Chem. Front.* **2018**, *2* (4), 700–703.

(100) Dai, S.; Zhao, F.; Zhang, Q.; Lau, T.-K.; Li, T.; Liu, K.; Ling, Q.; Wang, C.; Lu, X.; You, W.; Zhan, X. Fused Nonacyclic Electron Acceptors for Efficient Polymer Solar Cells. *J. Am. Chem. Soc.* **2017**, *139* (3), 1336–1343.

(101) Li, Z.; Dai, S.; Xin, J.; Zhang, L.; Wu, Y.; Rech, J.; Zhao, F.; Li, T.; Liu, K.; Liu, Q.; Ma, W.; You, W.; Wang, C.; Zhan, X. Enhancing the Performance of the Electron Acceptor ITIC-Th *via* Tailoring Its End Groups. *Mater. Chem. Front.* **2018**, *2* (3), 537–543.

(102) Zhao, W.; Li, S.; Yao, H.; Zhang, S.; Zhang, Y.; Yang, B.; Hou, J. Molecular Optimization Enables over 13% Efficiency in Organic Solar Cells. *J. Am. Chem. Soc.* **2017**, *139* (21), 7148–7151.

(103) Yuan, J.; Zhang, Y.; Zhou, L.; Zhang, G.; Yip, H.-L.; Lau, T.-K.; Lu, X.; Zhu, C.; Peng, H.; Johnson, P. A.; Leclerc, M.; Cao, Y.; Ulanski, J.; Li, Y.; Zou, Y. Single-Junction Organic Solar Cell with over 15% Efficiency Using Fused-Ring Acceptor with Electron-Deficient Core. *Joule* **2019**, DOI: 10.1016/j.joule.2019.01.004.

(104) Aldrich, T. J.; Matta, M.; Zhu, W.; Swick, S. M.; Stern, C. L.; Schatz, G. C.; Facchetti, A.; Melkonyan, F. S.; Marks, T. J. Fluorination Effects on Indacenodithienothiophene Acceptor Packing and Electronic Structure, End-Group Redistribution, and Solar Cell Photovoltaic Response. *J. Am. Chem. Soc.* **2019**, *141* (7), 3274–3287.

(105) Lakhwani, G.; Rao, A.; Friend, R. H. Bimolecular Recombination in Organic Photovoltaics. *Annu. Rev. Phys. Chem.* **2014**, *65* (1), 557–581.

(106) Li, W.; Albrecht, S.; Yang, L.; Roland, S.; Tumbleston, J. R.; McAfee, T.; Yan, L.; Kelly, M. A.; Ade, H.; Neher, D.; You, W. Mobility-Controlled Performance of Thick Solar Cells Based on Fluorinated Copolymers. *J. Am. Chem. Soc.* **2014**, *136* (44), 15566–15576.

(107) Würfel, U.; Neher, D.; Spies, A.; Albrecht, S. Impact of Charge Transport on Current–voltage Characteristics and Power-Conversion Efficiency of Organic Solar Cells. *Nat. Commun.* **2015**, *6* (1), 6951.

(108) Bartesaghi, D.; Pérez, I. del C.; Kniepert, J.; Roland, S.; Turbiez, M.; Neher, D.; Koster, L. J. A. Competition between Recombination and Extraction of Free Charges Determines the Fill Factor of Organic Solar Cells. *Nat. Commun.* **2015**, *6* (1), 7083.

(109) Bartelt, J. A.; Lam, D.; Burke, T. M.; Sweetnam, S. M.; McGehee, M. D. Charge-Carrier Mobility Requirements for Bulk Heterojunction Solar Cells with High Fill Factor and External Quantum Efficiency >90%. *Adv. Energy Mater.* **2015**, *5* (15), 1500577.

(110) Chen, P.; Shi, S.; Wang, H.; Qiu, F.; Wang, Y.; Tang, Y.; Feng, J.-R.; Guo, H.; Cheng, X.; Guo, X. Aggregation Strength Tuning in Difluorobenzoxadiazole-Based Polymeric Semiconductors for High-Performance Thick-Film Polymer Solar Cells. *ACS Appl. Mater. Interfaces* **2018**, *10* (25), 21481–21491.

(111) Mukherjee, S.; Proctor, C. M.; Bazan, G. C.; Nguyen, T.-Q.; Ade, H. Significance of Average Domain Purity and Mixed Domains on the Photovoltaic Performance of High-Efficiency Solution-Processed Small-Molecule BHJ Solar Cells. *Adv. Energy Mater.* **2015**, *5* (21), 1500877.

(112) Zhou, H.; Yang, L.; Liu, S.; You, W. A Tale of Current and Voltage: Interplay of Band Gap and Energy Levels of Conjugated Polymers in Bulk Heterojunction Solar Cells. *Macromolecules* **2010**, *43* (24), 10390–10396.